



**HAL**  
open science

# On the Identifiability of Transform Learning for Non-negative Matrix Factorization

Sixin Zhang, Emmanuel Soubies, Cédric Févotte

► **To cite this version:**

Sixin Zhang, Emmanuel Soubies, Cédric Févotte. On the Identifiability of Transform Learning for Non-negative Matrix Factorization. *IEEE Signal Processing Letters*, 2020, 10.1109/LSP.2020.3020431 . hal-02542653v4

**HAL Id: hal-02542653**

**<https://hal.science/hal-02542653v4>**

Submitted on 2 Jul 2022 (v4), last revised 23 Aug 2022 (v5)

**HAL** is a multi-disciplinary open access archive for the deposit and dissemination of scientific research documents, whether they are published or not. The documents may come from teaching and research institutions in France or abroad, or from public or private research centers.

L'archive ouverte pluridisciplinaire **HAL**, est destinée au dépôt et à la diffusion de documents scientifiques de niveau recherche, publiés ou non, émanant des établissements d'enseignement et de recherche français ou étrangers, des laboratoires publics ou privés.

# Leveraging Joint-Diagonalization in Transform-Learning NMF

Sixin Zhang, *Member, IEEE*, Emmanuel Soubies, *Member, IEEE*, and Cédric Févotte, *Fellow, IEEE*

**Abstract**—Non-negative matrix factorization with transform learning (TL-NMF) is a recent idea that aims at learning data representations suited to NMF. In this work, we relate TL-NMF to the classical matrix joint-diagonalization (JD) problem. We show that, when the number of data realizations is sufficiently large, TL-NMF can be replaced by a two-step approach—termed as JD+NMF—that estimates the transform through JD, prior to NMF computation. In contrast, we found that when the number of data realizations is limited, not only is JD+NMF no longer equivalent to TL-NMF, but the inherent low-rank constraint of TL-NMF turns out to be an essential ingredient to learn meaningful transforms for NMF.

**Index Terms**—Transform learning, Nonnegative matrix factorization, Joint-diagonalization, Statistical estimation, Nonconvex optimization, Quasi-Newton method.

## I. INTRODUCTION

LET  $\mathbf{Y} \in \mathbb{R}^{M \times N}$  be a random matrix that satisfies the following moment conditions:  $\forall(m', m, n)$ ,

$$\begin{cases} \mathbb{E}([\bar{\Phi}\mathbf{Y}]_{mn}) = 0, & (\text{mean}) \\ \mathbb{E}([\bar{\Phi}\mathbf{Y}]_{mn}^2) = [\bar{\mathbf{W}}\bar{\mathbf{H}}]_{mn}, & (\text{variance}) \\ \mathbb{E}([\bar{\Phi}\mathbf{Y}]_{mn}[\bar{\Phi}\mathbf{Y}]_{m'n'}) = 0, & (\text{covariance}) \end{cases} \quad (1)$$

where  $\bar{\Phi} \in \mathbb{R}^{M \times M}$  is an orthogonal matrix and  $\bar{\mathbf{W}} \in \mathbb{R}_+^{M \times \bar{K}}$ ,  $\bar{\mathbf{H}} \in \mathbb{R}_+^{\bar{K} \times N}$  are two nonnegative matrices such that  $[\bar{\mathbf{W}}\bar{\mathbf{H}}]_{mn} > 0$ . Here  $\bar{K}$  denotes the non-negative rank of  $\bar{\mathbf{W}}\bar{\mathbf{H}}$  [1]. These fairly general conditions encompass, for instance, the popular Gaussian composite model (GCM) [2], [3], which reads as

$$[\bar{\Phi}\mathbf{Y}]_{mn} \underset{\text{i.i.d.}}{\sim} \mathcal{N}(0, [\bar{\mathbf{W}}\bar{\mathbf{H}}]_{mn}), \quad \forall(m, n), \quad (2)$$

where  $\mathcal{N}$  denotes the real-valued Gaussian distribution.

In this paper, we are concerned with the problem of estimating the triplet  $(\bar{\Phi}, \bar{\mathbf{W}}, \bar{\mathbf{H}})$  from  $S$  i.i.d. realizations of  $\mathbf{Y}$ , which we denote by  $\{\mathbf{Y}^{(s)}\}_{s=1}^S$  (this includes the most frequent scenario  $S = 1$ ). In the literature, this problem is referred to as transform-learning nonnegative matrix factorization (TL-NMF) [4], [5] and is also a special case of independent low-rank tensor analysis (ILRTA) [6]. When the columns of  $\mathbf{Y}$  are composed of overlapping segments of a temporal signal and  $\bar{\Phi}$  is a fixed frequency-transform matrix such as the DCT (we only consider real-valued transforms in this paper), the product  $\bar{\Phi}\mathbf{Y}$  defines a short-time frequency transform. Its power values  $[\bar{\Phi}\mathbf{Y}]_{mn}^2$  define a *spectrogram*.

The authors are with IRIT, Université de Toulouse, CNRS, Toulouse, France. Email: firstname.lastname@irit.fr. This work was supported by the European Research Council (ERC FACTORY-CoG-6681839), the French National Research Agency (ANR ANITI-3IA) and the National Research Foundation in Singapore (CREATE project DesCartes).

Equation (1) dictates that the spectrogram is given in expectation by the nonnegative matrix factorization (NMF)  $\bar{\mathbf{W}}\bar{\mathbf{H}}$ . The zero-mean assumption is valid for centered temporal signals such as audio signals. The zero-covariance assumption is a working assumption that reflects uncorrelation of the transform coefficients. The dictionary matrix  $\bar{\mathbf{W}}$  captures meaningful spectral patterns while the activation matrix  $\bar{\mathbf{H}}$  describes how the spectral samples are decomposed onto the dictionary.

NMF has found a large range of applications in audio signal processing, such as source separation or music transcription [3], [7], [8], [9]. In TL-NMF, the fixed transform assumption is relaxed and  $\bar{\Phi}$  is estimated together with  $\bar{\mathbf{W}}$  and  $\bar{\mathbf{H}}$  [4]. This was shown to lead in some cases to more meaningful representations. For example, it was shown in [6] that better source separation performance can be achieved with adaptive learned transform. In [5], it was shown that learning  $\bar{\Phi}$  allows to capture harmonic atoms with fundamental frequencies that precisely match the music notes in the data, when a DCT transform can only abide by a fixed frequency grid. TL-NMF was inspired by works about learning sparsifying transforms [10] and to a lesser extent independent component analysis (ICA) [11], [12].

TL-NMF can be tackled through the resolution of the following optimization problem

$$(\Phi^*, \mathbf{W}^*, \mathbf{H}^*) \in \underset{\substack{\Phi \in \mathcal{O}(M) \\ (\mathbf{W}, \mathbf{H}) \in F_K}}{\arg \min}} C_S(\Phi, \mathbf{W}, \mathbf{H}), \quad (3)$$

where  $\mathcal{O}(M)$  denotes the real orthogonal matrix group on  $\mathbb{R}^M$  and  $F_K \subset \mathbb{R}_+^{M \times K} \times \mathbb{R}_+^{K \times N}$  is a constraint set for the nonnegative matrices  $\mathbf{W}$  and  $\mathbf{H}$  which will be made explicit later. Here  $K$  represents the factorization rank whose choice depends on the considered dataset and application [9], [13]. The objective function  $C_S$  in (3) is defined by

$$C_S(\Phi, \mathbf{W}, \mathbf{H}) = \sum_{m,n=1}^{M,N} \frac{\mathbb{E}_S([\Phi\mathbf{Y}]_{mn}^2) + \epsilon_0}{[\mathbf{W}\mathbf{H}]_{mn} + \epsilon_0} + \log([\mathbf{W}\mathbf{H}]_{mn} + \epsilon_0) \quad (4)$$

where  $\mathbb{E}_S([\Phi\mathbf{Y}]_{mn}^2)$  is a consistent estimator of  $\mathbb{E}([\Phi\mathbf{Y}]_{mn}^2)$  computed from the  $S$  i.i.d. realizations  $\{\mathbf{Y}^{(s)}\}_{s=1}^S$ , and  $\epsilon_0 \geq 0$ .

- The rationale behind the choice of Problem (3) is that, when
- i)  $S = \infty$  (i.e.,  $\mathbb{E}_S([\Phi\mathbf{Y}]_{mn}^2) = \mathbb{E}([\Phi\mathbf{Y}]_{mn}^2)$ ), and  $\epsilon_0 = 0$ ,
  - ii)  $K \geq \bar{K}$  (i.e., the NMF rank  $K$  in (3) is larger than  $\bar{K}$ , the true rank in model (1)),

each global minimizer  $(\Phi^*, \mathbf{W}^*, \mathbf{H}^*)$  of  $C_S$  is such that the rows of  $\Phi^*$  and  $\bar{\Phi}$  span the same subspaces (we say that  $\bar{\Phi}$  is identifiable by solving (3)) and  $\mathbf{W}^*\mathbf{H}^* = \bar{\mathbf{W}}\bar{\mathbf{H}}$  [5]. Moreover,

under the GCM,  $C_S$  corresponds to the expected negative log-likelihood of  $\mathbf{Y}$  conditioned to  $(\Phi, \mathbf{W}, \mathbf{H})$ .

*Contributions and Outline:* This identifiability result relies on a key property of  $C_S$  that is, in the regime  $S = \infty$  and  $K \geq \bar{K}$ ,

$$\forall \Phi \in \mathcal{O}(M), \min_{(\mathbf{W}, \mathbf{H}) \in F_K} C_S(\Phi, \mathbf{W}, \mathbf{H}) = L_S(\Phi), \quad (5)$$

where  $L_S$  is related to the joint-diagonalization (JD) criterion derived in [14] (and formally defined in Section II).

This suggests the following two-step alternative to Problem (3)

$$\begin{aligned} \Phi^\bullet &\in \arg \min_{\Phi \in \mathcal{O}(M)} L_S(\Phi), \\ (\mathbf{W}^\bullet, \mathbf{H}^\bullet) &\in \arg \min_{(\mathbf{W}, \mathbf{H}) \in F_K} C_S(\Phi^\bullet, \mathbf{W}, \mathbf{H}), \end{aligned} \quad (6)$$

which we refer to as JD+NMF. Although it is straightforward from (5) that problems (3) and (6) are equivalent in the ideal case  $S = \infty$  and  $\epsilon_0 = 0$ , their relation in the more practical situation  $S < \infty$  and  $\epsilon_0 > 0$  (usually required for numerical stability) needs to be analyzed. In particular:

- How does (6) deviate from (3) with respect to (w.r.t.)  $S$ ?
- Is one of these two formulations preferable from an optimization perspective? (quality of the reached local minimizer, convergence speed)

The main contribution of this work is to provide theoretical and numerical insights to these questions. In Section II, we set out the basic assumptions and definitions required for our analysis and prove in Theorem 1 that both TL-NMF (Problem (3)) and JD+NMF (Problem (6)) admit at least one solution. Then, Section III is dedicated to the characterization of the closeness between the solution sets of these two problems. We first identify in Theorem 2 quantities that allow to characterize three regimes where the solution sets of TL-NMF and JD+NMF are i) disjoint, ii) partially intersecting, and iii) equal, respectively. Then, by analyzing the asymptotic behavior (w.r.t.  $S$ ) of these key quantities, we show that with high probability, the gaps between the two solution sets converge to zero (in terms of the Itakua-Saito divergence [15], [2]) as  $S$  grows (Proposition 2 and Theorem 3). Under the GCM, we further prove in Theorem 4 that the rate of convergence is at least of the order of  $O(1/S)$ . In Section IV, we adapt existing TL-NMF and JD minimization algorithms to Problems (3) and (6) as they come with slightly different objective functions and constraint sets. Finally, in Section V, we deploy these algorithms to illustrate and complement numerically our theoretical findings (tightness of the expected asymptotic behavior, behavior when  $S$  is small).

*Notations:* For a matrix  $\mathbf{X} \in \mathbb{R}^{M \times N}$ , we denote by  $\mathbf{x}_n$ ,  $\mathbf{x}_m$  and  $[\mathbf{X}]_{mn}$  (or  $x_{mn}$ ) its  $n$ -th column,  $m$ -th row, and  $(m, n)$ -th element, respectively. Moreover, we use the notation  $|\mathbf{X}|^{\circ 2}$  for its element-wise modulus square. For a vector  $\mathbf{y} \in \mathbb{R}^T$ ,  $\mathbf{y}[t]$  denotes its  $t$ -th element and  $\mathbf{y}^\top$  denotes its transpose. We write  $\text{Diag}(\mathbf{y})$  for the diagonal matrix formed out of the vector  $\mathbf{y}$ , and  $\text{Diag}(\mathbf{X})$  for the vector formed by the diagonal elements of  $\mathbf{X}$ . Finally,  $X_n \xrightarrow{P} X$  stands for the convergence in probability of the sequence  $\{X_n\}_n$  of random variables toward the random variable  $X$ .

## II. PRELIMINARIES

### A. Definitions and Useful Results

First, from now on, and throughout the paper, we set  $\epsilon_0 > 0$ . Then, let us provide a reformulation of the moment conditions in (1) that will be relevant in our analysis.

**Proposition 1.** *The moment conditions (1) can be equivalently expressed as*

$$\mathbb{E}(\mathbf{y}_n) = \mathbf{0}, \quad (7)$$

$$\bar{\Phi} \Sigma_n \bar{\Phi}^\top = \text{Diag}(\bar{\mathbf{W}} \bar{\mathbf{h}}_n), \quad (8)$$

where  $\Sigma_n = \mathbb{E}(\mathbf{y}_n \mathbf{y}_n^\top)$  denotes the covariance matrix of the  $n$ -th column of  $\mathbf{Y}$ .

*Proof.* The mean condition in (1) implies that for any  $n$ ,  $\mathbb{E}(\bar{\Phi} \mathbf{y}_n) = \mathbf{0}$ , thus we have  $\mathbb{E}(\mathbf{y}_n) = \mathbf{0}$  due to the invertibility of  $\bar{\Phi}$ . The variance condition implies that the diagonal terms of  $\bar{\Phi} \Sigma_n \bar{\Phi}^\top$  equal to the vector  $\bar{\mathbf{W}} \bar{\mathbf{h}}_n$ . This is because, by definition,  $[\bar{\Phi} \Sigma_n \bar{\Phi}^\top]_{mm} = [\bar{\mathbf{W}} \mathbf{H}]_{mn} = (\bar{\mathbf{W}} \bar{\mathbf{h}}_n)[m]$ . Similarly, the covariance condition implies that the off-diagonal terms of  $\bar{\Phi} \Sigma_n \bar{\Phi}^\top$  are zero.  $\square$

Finally, to complete the formulation of Problems (3) and (6) we define below the constraint set  $F_K$  as well as the empirical expectation operator  $\mathbb{E}_S(\cdot)$  used in the definition of  $C_S$  in (3).

*Constraint Set:* we define the constraint set  $F_K$  as

$$F_K = \{(\mathbf{W}, \mathbf{H}) \in \mathbb{R}_+^{M \times K} \times \mathbb{R}_+^{K \times N} \mid \forall k, \|\mathbf{w}_k\|_1 = 1\}, \quad (9)$$

on which  $C_S$  is well-defined (i.e., no singularity) when  $\epsilon_0 > 0$ . The normalization constraint on each column of  $\mathbf{W}$  allows to break the scaling ambiguity between  $\mathbf{W}$  and  $\mathbf{H}$ . It is worth mentioning that there are other types ambiguities in NMF [16], [9]. These include permutations of the columns of  $\mathbf{W}$  and rows of  $\mathbf{H}$ , or local nonnegativity-preserving rotations. Yet, considering the scaling ambiguity turns out to be an important ingredient to prove the existence of a solution to TL-NMF and JD+NMF (see the proof of Theorem 1 in Appendix B). This motivates the definition of  $F_K$  in (9).

*Empirical Expectation:* We consider the empirical expectation of  $[\Phi \mathbf{Y}]_{mn}^2$ , that is

$$\mathbb{E}_S([\Phi \mathbf{Y}]_{mn}^2) = \frac{1}{S} \sum_{s=1}^S [\Phi \mathbf{Y}^{(s)}]_{mn}^2. \quad (10)$$

Moreover, we use the notation  $\mathbb{E}_S(|\Phi \mathbf{Y}|^{\circ 2})$  to refer to the point-wise empirical expectation, i.e.,  $[\mathbb{E}_S(|\Phi \mathbf{Y}|^{\circ 2})]_{mn} = \mathbb{E}_S([\Phi \mathbf{Y}]_{mn}^2)$ . Finally, we introduce the following empirical covariance matrix:

$$\Sigma_{n,S} = \frac{1}{S} \sum_{s=1}^S \mathbf{y}_n^{(s)} (\mathbf{y}_n^{(s)})^\top. \quad (11)$$

### B. From TL-NMF to JD+NMF

For any integer  $S > 0$ , one can easily verify the following decomposition of the TL-NMF objective in (4),

$$C_S(\Phi, \mathbf{W}, \mathbf{H}) = L_S(\Phi) + I_S(\Phi, \mathbf{W}, \mathbf{H}), \quad (12)$$

with  $L_S$  and  $I_S$  defined by

$$L_S(\Phi) = MN + \sum_{m,n=1}^{M,N} \log(\mathbb{E}_S([\Phi\mathbf{Y}]_{mn}^2) + \epsilon_0), \quad (13)$$

$$I_S(\Phi, \mathbf{W}, \mathbf{H}) = D_{\epsilon_0}(\mathbb{E}_S(|\Phi\mathbf{Y}|^{\circ 2})|\mathbf{W}\mathbf{H}), \quad (14)$$

where  $D_{\epsilon_0}(\cdot|\cdot)$  denotes a regularized form of the Itakura-Saito (IS) divergence. For two non-negative matrices  $\mathbf{A}$  and  $\mathbf{B}$ , it is defined by

$$D_{\epsilon_0}(\mathbf{A}|\mathbf{B}) = \sum_{m,n} \left( \frac{[\mathbf{A}]_{mn} + \epsilon_0}{[\mathbf{B}]_{mn} + \epsilon_0} - \log \left( \frac{[\mathbf{A}]_{mn} + \epsilon_0}{[\mathbf{B}]_{mn} + \epsilon_0} \right) - 1 \right). \quad (15)$$

The term  $I_S$  in (14) is related to Itakura-Saito NMF (IS-NMF) [2]. Indeed, when  $\Phi$  is fixed, the minimization of  $I_S$  with respect to  $(\mathbf{W}, \mathbf{H}) \in F_K$  produces a NMF of  $\mathbb{E}_S(|\Phi\mathbf{Y}|^{\circ 2})$  where the fit is measured by the IS divergence.

The term  $L_S$  is related to joint-diagonalization (JD), as specified by Lemma 1.

**Lemma 1.** *For all  $\Phi \in \mathcal{O}(M)$ ,*

$$L_S(\Phi) = MN + \sum_{n=1}^N \log \det \text{Diag}(\Phi(\Sigma_{n,S} + \epsilon_0 \mathbf{I})\Phi^\top), \quad (16)$$

which corresponds, up to a constant term, to the JD criterion derived in [14].

*Proof.* See Appendix A.  $\square$

The minimization of  $L_S$  over  $\mathcal{O}(M)$  leads to an orthogonal matrix  $\Phi$  such that  $\Phi\Sigma_{n,S}\Phi^\top$  is as diagonal as possible. The additional diagonal matrix  $\epsilon_0 \mathbf{I}$  in (16) can be interpreted (up to a constant normalization) as a linear shrinkage estimator for covariance matrix estimation [17].

Hence, from the decomposition (12), TL-NMF can be interpreted as a trade-off between the JD of the covariance matrices  $\{\Sigma_{n,S}\}_n$  and the NMF of the variance matrix  $\mathbb{E}_S(|\Phi\mathbf{Y}|^{\circ 2})$ . In contrast, the alternative scheme (6) attempts to achieve the same goal in a two-step fashion by first solving a JD problem to obtain  $\Phi^\bullet$  and then solving an IS-NMF problem given  $\Phi^\bullet$  to get  $(\mathbf{W}^\bullet, \mathbf{H}^\bullet)$ .

**Remark 1.** *From Lemma 1, one can see that the “regularization” parameter  $\epsilon_0 > 0$  ensures that  $L_S$  is continuous over  $\mathcal{O}(M)$ . Indeed, when  $S < M$ ,  $\Sigma_{n,S}$  have vanishing eigenvalues meaning that some diagonal entries of  $\Phi\Sigma_{n,S}\Phi^\top$  may be zero. Hence, taking  $\epsilon_0 > 0$  ensures that all the log-terms of (16) are non-degenerate.*

**Remark 2.** *The JD criterion derived in [14] and essentially given by (16) does not assume  $\Phi$  to be explicitly orthogonal but merely non-singular. Many orthogonal JD algorithms were designed in the early age of ICA when whitening was still a standard data pre-processing step. A seminal example is the Jacobi algorithm by Cardoso and Souloumiac [18] for JD with a least-squares criterion. However, to ensure optimal one-step performance [19], the whitening step was eventually dropped in the ICA community. Non-orthogonal JD became the mainstream, and many algorithms ensued for various*

*criteria (such as based on least-squares, maximum likelihood or information measures), see, e.g., [20], [21], [22], [23], [24]. More recently, [25] leverages Riemannian optimization to unify many existing methods and introduce new ones under various constraints for  $\Phi$ .*

*In this work, we restrict  $\Phi$  to be orthogonal because TL-NMF aims to generalize short-time frequency transforms for which orthogonality is somehow natural or desired. Moreover when  $S = \infty$ , we showed that the row subspaces of  $\bar{\Phi}$  are identifiable [5]. Such an analysis is more difficult in the general case (see [26], [27] for related discussions). Still, removing the orthogonality assumption of  $\Phi$  could be beneficial in practice and forms a relevant research direction (see further discussion in Section VI).*

### III. RELATIONSHIP BETWEEN JD+NMF AND TL-NMF

#### A. Existence of a Solution

Before analyzing the relation between TL-NMF and JD+NMF, it is worth checking that they both admit at least one solution. To the best of our knowledge, this question has never been addressed in the TL-NMF literature, nor in NMF literature (i.e., existence of global minimizer(s) for  $I_S$ , see Lemma 3).

**Theorem 1.** *The solution sets  $\Omega^*$  of TL-NMF (Problem (3)) and  $\Omega^\bullet$  of JD+NMF (Problem (6)) are nonempty and compact.*

*Proof.* See Appendix B.  $\square$

**Remark 3.** *The assumption  $\epsilon_0 > 0$  is necessary for the functions  $L_S$  and  $I_S$  to be well-defined and to show the existence of solutions to TL-NMF and JD+NMF. We chose to include  $\epsilon_0$  in the definitions of  $L_S$  and  $I_S$  but we could alternatively have set  $\epsilon_0 = 0$  in  $L_S$  and  $I_S$ , and add an inequality of the form  $\mathbf{W}\mathbf{H} \geq \epsilon_0$  in the constraint set  $F_K$ . This is related to the approach followed by [28] to study the convergence of NMF with a large range of divergences (including the generalized Kullback-Leibler divergence [29]) under constraints of the form  $\mathbf{W} \geq \epsilon_0, \mathbf{H} \geq \epsilon_0$ .*

#### B. When does JD+NMF meet TL-NMF?

In Theorem 2, we characterize the closeness between the solutions of JD+NMF and the solutions of TL-NMF. A graphical illustration of this result is depicted in Figure 1.

**Theorem 2.** *Let  $\Omega^*$  and  $\Omega^\bullet$  be defined as in Theorem 1. Define*

$$\underline{\lambda}^* = \min_{(\Phi, \mathbf{W}, \mathbf{H}) \in \Omega^*} I_S(\Phi, \mathbf{W}, \mathbf{H}), \quad (17)$$

$$\bar{\lambda}^* = \max_{(\Phi, \mathbf{W}, \mathbf{H}) \in \Omega^*} I_S(\Phi, \mathbf{W}, \mathbf{H}), \quad (18)$$

and similarly  $\underline{\lambda}^\bullet$  and  $\bar{\lambda}^\bullet$  by replacing  $\Omega^*$  by  $\Omega^\bullet$ . Then,

$$0 \leq \underline{\lambda}^* \leq \bar{\lambda}^* \leq \underline{\lambda}^\bullet \leq \bar{\lambda}^\bullet < +\infty. \quad (19)$$

Moreover,

$$\Omega^\bullet \cap \Omega^* \neq \emptyset \iff \bar{\lambda}^* = \underline{\lambda}^\bullet, \quad (20)$$

$$\Omega^\bullet = \Omega^* \iff \underline{\lambda}^* = \bar{\lambda}^\bullet. \quad (21)$$

*Proof.* See Appendix C.  $\square$

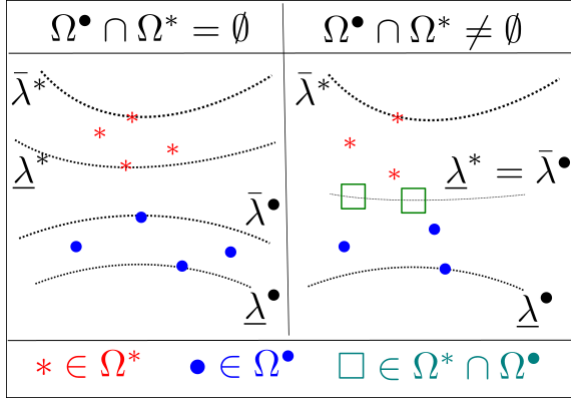


Fig. 1. Graphical illustration of Theorem 2. The relationship between the solutions sets  $\Omega^*$  and  $\Omega^\bullet$  of TL-NMF and JD+NMF is described in terms of specific level lines of  $I_S$ . Note that we represented here  $\Omega^*$  and  $\Omega^\bullet$  as countable sets for the sake of illustration, but they may not be.

There are at least two situations where JD+NMF is equivalent to TL-NMF (i.e., (21) is satisfied):

- $S = \infty$  and  $K \geq \bar{K}$ ,
- $S < \infty$  and  $K \geq \min\{M, N\}$ .

Indeed, in these two cases we have that,  $\forall \Phi \in \mathcal{O}(M)$ ,

$$\exists (\mathbf{W}, \mathbf{H}) \in F_K, \text{ such that } \mathbb{E}_S(|\Phi \mathbf{Y}|^{\circ 2}) = \mathbf{W}\mathbf{H}, \quad (22)$$

i.e., there exists an exact factorization of  $\mathbb{E}_S(|\Phi \mathbf{Y}|^{\circ 2})$ . When  $K \geq \min\{M, N\} = N$  it suffices to populate  $\mathbf{W}$  with  $\mathbb{E}_S(|\Phi \mathbf{Y}|^{\circ 2})$ ,  $\mathbf{H}$  with  $\mathbf{I}_N$ , and to complete with zeros. A similar exact factorization can be obtained when  $K \geq \min\{M, N\} = M$  by switching the roles of  $\mathbf{W}$  and  $\mathbf{H}$ . For the case  $S = \infty$ , we refer the reader to the proof of Proposition 2 in Appendix D. Consequently, in such cases, we get from (22) that

$$\forall \Phi \in \mathcal{O}(M), \min_{(\mathbf{W}, \mathbf{H}) \in F_K} I_S(\Phi, \mathbf{W}, \mathbf{H}) = 0. \quad (23)$$

It then follows from (3) (resp., (6)) and (12) that

$$\forall (\Phi, \mathbf{W}, \mathbf{H}) \in \Omega^* \text{ (resp., } \Omega^\bullet), I_S(\Phi, \mathbf{W}, \mathbf{H}) = 0 \quad (24)$$

and thus  $\underline{\lambda}^* = \bar{\lambda}^\bullet = 0$ .

The situation is more involved when  $S < \infty$  and  $K < \min\{M, N\}$ . In this case, we get from Theorem 2 that the closeness between the solutions of JD+NMF and TL-NMF is controlled by the inner  $\underline{\lambda}^\bullet - \bar{\lambda}^*$  and the outer  $\bar{\lambda}^\bullet - \underline{\lambda}^*$  gaps. Indeed, by definition, we get that for any  $(\Phi^*, \mathbf{W}^*, \mathbf{H}^*) \in \Omega^*$  and  $(\Phi^\bullet, \mathbf{W}^\bullet, \mathbf{H}^\bullet) \in \Omega^\bullet$ ,

$$0 \leq \underline{\lambda}^\bullet - \bar{\lambda}^* \leq I_S^\bullet - I_S^* \leq \bar{\lambda}^\bullet - \underline{\lambda}^*, \quad (25)$$

where  $I_S^\bullet = I_S(\Phi^\bullet, \mathbf{W}^\bullet, \mathbf{H}^\bullet)$  and  $I_S^* = I_S(\Phi^*, \mathbf{W}^*, \mathbf{H}^*)$ . Moreover, one can see that the outer gap also controls the proximity between minimizers in terms of  $C_S$  values because

$$0 \leq C_S^\bullet - C_S^* \leq I_S^\bullet - I_S^* \leq \bar{\lambda}^\bullet - \underline{\lambda}^*, \quad (26)$$

where the first inequality is obtained by combining (12) with the fact that  $L_S^\bullet \leq L_S^*$ . Note that here,  $C_S^\bullet$  and  $C_S^*$  (resp.,  $L_S^\bullet$ , and  $L_S^*$ ) are the counterparts of  $I_S^\bullet$  and  $I_S^*$  for the objectives  $C_S$  (resp.,  $L_S$ ). In Section III-C, we shall analyse

the asymptotic behaviour of the inner and outer gaps.

Finally, let us emphasize that the inequalities (19) also reveal that the transforms  $\Phi^\bullet$  obtained by JD+NMF are *at best* as amenable to NMF (in terms of IS-divergence) as any  $\Phi^*$  learned by TL-NMF.

**Remark 4.** *The above discussion about the quality of the learned  $\Phi$  in terms of  $I_S$  values may raise the following question: why not directly minimizing  $I_S$  with respect to  $(\Phi, \mathbf{W}, \mathbf{H})$ ? The latter approach was in particular the one considered in the original TL-NMF paper [4] (with an additional sparsity-enforcing term for  $\mathbf{H}$ ), an arbitrary choice inherited from IS-NMF [30]. As a matter of fact, in light of our results, several arguments play in favor of minimizing  $C_S$  rather than  $I_S$ . First, under the GCM,  $C_S$  comes with a probabilistic interpretation (log-likelihood function). Second, when  $S = \infty$ , there exist  $(\mathbf{W}, \mathbf{H})$  such that  $I_S(\Phi, \mathbf{W}, \mathbf{H}) = 0$  for all  $\Phi$  (see (23)). This means that  $I_S$  does not constitute a good measure to discriminate the  $\Phi$ . In contrast, the minimization of  $C_S$  allows to identify the true transform  $\bar{\Phi}$  (the term  $L_S(\Phi)$  acts somehow as a penalization term) [5]. Lastly, this ability to learn meaningful transform (e.g., close to  $\bar{\Phi}$ ) by minimizing  $C_S$  appears to be also true when  $S$  is small (see Section V-D).*

### C. Asymptotic Analysis

In this section we analyze the closeness between JD+NMF and TL-NMF when  $S < \infty$  and  $K \in [\bar{K}, \min\{M, N\}]$ .<sup>1</sup> We derive a sufficient condition under which the outer gap  $\bar{\lambda}^\bullet - \underline{\lambda}^*$  (and consequently the inner gap  $\underline{\lambda}^\bullet - \bar{\lambda}^*$ ) converges (in probability) to zero as  $S$  grows. Given that

$$\underline{\lambda}^\bullet - \bar{\lambda}^* \leq \bar{\lambda}^\bullet - \underline{\lambda}^* \leq \bar{\lambda}^\bullet, \quad (27)$$

we first provide in Proposition 2 an upper bound of  $\bar{\lambda}^\bullet$  that is independent of the solution sets  $\Omega^*$  and  $\Omega^\bullet$ .

**Proposition 2.** *Under condition (1) and  $K \geq \bar{K}$ , we have for all  $S > 0$ ,*

$$\bar{\lambda}^\bullet \leq \max_{\Phi \in \mathcal{O}(M)} Q_S(\Phi) \quad (28)$$

where

$$Q_S(\Phi) = D_{e_0}(\mathbb{E}_S(|\Phi \mathbf{Y}|^{\circ 2}) | \mathbb{E}(|\Phi \mathbf{Y}|^{\circ 2})). \quad (29)$$

*Proof.* See Appendix D.  $\square$

We now derive in Theorem 3 a sufficient condition for the upper bound  $\max_{\Phi} Q_S(\Phi)$  to converge to zero in probability.

**Theorem 3.** *Assume that the empirical estimator  $\mathbb{E}_S(|\Phi \mathbf{Y}|^{\circ 2})$  converges uniformly toward  $\mathbb{E}(|\Phi \mathbf{Y}|^{\circ 2})$  in probability, i.e.,*

$$\max_{(m,n)} \max_{\Phi \in \mathcal{O}(M)} \left| \mathbb{E}_S(|\Phi \mathbf{Y}|_{mn}^2) - \mathbb{E}(|\Phi \mathbf{Y}|_{mn}^2) \right| \xrightarrow{P} 0, \quad (30)$$

Then

$$\max_{\Phi \in \mathcal{O}(M)} Q_S(\Phi) \xrightarrow{P} 0 \text{ as } S \rightarrow \infty. \quad (31)$$

*Proof.* See Appendix E.  $\square$

<sup>1</sup>The more intricate case  $K < \bar{K}$  is not considered in the paper.

Under the GCM, we can go one step further than Theorem 3 by deriving the convergence rate of  $\max_{\Phi} Q_S(\Phi)$ .

**Theorem 4.** *Under GCM defined by (2), condition (30) is always satisfied. Moreover, for  $t > 0$  and  $S$  large enough such that  $h_S = 3\frac{\sqrt{M+t}}{\sqrt{S}} < 1$ , we have*

$$\max_{\Phi \in \mathcal{O}(M)} Q_S(\Phi) < MN \frac{h_S^2}{1 - h_S}, \quad (32)$$

with probability at least  $(1 - 2e^{-t^2/2})^N$ .

*Proof.* See Appendix E.  $\square$

It is worth mentioning that the proof of Theorem 4 makes use of existing results on covariance matrix estimation [31] which can be generalized to the case where the entries of  $\mathbf{Y}$  follow some sub-Gaussian distributions [32].

**Remark 5.** *From Theorem 4, we get that with high probability, as  $S$  grows,  $\max_{\Phi} Q_S(\Phi)$  converges at least at a rate of  $O(1/S)$ . Indeed, for any  $t > 0$ , there exists  $S^*$  such that for all  $S \geq S^*$ ,  $h_S < 1$ . This means that for  $S$  sufficiently large, (32) holds with probability almost one. Then, the claim comes by observing that, for  $S$  large,  $h_S = O(1/\sqrt{S})$ .*

**Remark 6.** *We can provide insights on the tightness of the uniform bound (32) by analyzing a point-wise bound such as the asymptotic decay rate of  $Q_S(\bar{\Phi})$  with  $S$ . Let us first observe that*

$$Q_S(\bar{\Phi}) = \sum_{m,n=1}^{M,N} f(X_{mn}^{\bar{\Phi}}) \text{ for } X_{mn}^{\bar{\Phi}} = \frac{\mathbb{E}_S([\bar{\Phi}\mathbf{Y}]_{mn}^2) + \epsilon_0}{\mathbb{E}([\bar{\Phi}\mathbf{Y}]_{mn}^2) + \epsilon_0} \quad (33)$$

where  $f(x) = x - \log(x) - 1$ . Moreover, from (1), we get that  $\mathbb{E}([\bar{\Phi}\mathbf{Y}]_{mn}^2) > 0$  and, for  $S$  sufficiently large, we can assume that  $\mathbb{E}_S([\bar{\Phi}\mathbf{Y}]_{mn}^2) > 0$  (see discussion in Remark 1). Hence, we can set (for the purpose of this remark)  $\epsilon_0 = 0$ . We then get from the definition of  $\mathbb{E}_S$  in (10) that  $SX_{mn}^{\bar{\Phi}}$  follows a Chi-squared distribution  $\mathcal{X}_S$  of degree  $S$ . We deduce that

$$\begin{aligned} \mathbb{E}(f(X_{mn}^{\bar{\Phi}})) &= \frac{1}{S} \mathbb{E}(SX_{mn}^{\bar{\Phi}}) + \log(S) - \mathbb{E}(\log(SX_{mn}^{\bar{\Phi}})) - 1 \\ &= \log(S) - \psi(S/2) - \log(2) \end{aligned} \quad (34)$$

using the facts that  $\mathbb{E}(SX_{mn}^{\bar{\Phi}}) = S$  and  $\mathbb{E}(\log(SX_{mn}^{\bar{\Phi}})) = \psi(S/2) + \log(2)$  where  $\psi$  denotes the di-gamma function. Then, from the weak law of large number, we obtain that

$$\frac{1}{NM} Q_S(\bar{\Phi}) \xrightarrow[NM \rightarrow \infty]{P} (\log(S) - \psi(S/2) - \log(2)). \quad (35)$$

Noticing that, when  $S$  is large,  $\psi(S/2) \approx \log(S/2) - 1/S$ , we conclude (for  $M, N$  large and  $\epsilon_0 = 0$ ) that the decay rate of  $Q_S(\bar{\Phi})$  is of the order of  $O(1/S)$  which matches the uniform bound (32).

#### IV. OPTIMIZATION METHODS

To numerically address TL-NMF and JD+NMF problems, we deploy the alternating optimization methods outlined in Algorithms 1 and 2, respectively. They both rely on the standard *multiplicative updates* (MU) for the NMF factors  $\mathbf{W}, \mathbf{H}$ , and a quasi-Newton (QN) method for the update of

---

#### Algorithm 1 TL-NMF Solver

---

**In:**  $(J, J_{\text{NMF}}, J_{\text{TL}}) \in \mathbb{N}^3$ ,  $(\Phi_0, \mathbf{W}_0, \mathbf{H}_0) \in \mathcal{O}(M) \times F_K$

- 1: **for**  $j = 0 : J - 1$  **do**
- 2:    $(\mathbf{W}_{j+1}, \mathbf{H}_{j+1}) \leftarrow \text{MU}(C_S(\Phi_j, \cdot, \cdot); J_{\text{NMF}}, \mathbf{W}_j, \mathbf{H}_j)$
- 3:    $\Phi_{j+1} \leftarrow \text{QN}(C_S(\cdot, \mathbf{W}_{j+1}, \mathbf{H}_{j+1}); J_{\text{TL}}, \Phi_j)$
- 4: **end for**

**Out:**  $\Phi_J, \mathbf{W}_J, \mathbf{H}_J$

---



---

#### Algorithm 2 JD+NMF Solver

---

**In:**  $(J, J_{\text{NMF}}, J_{\text{TL}}) \in \mathbb{N}^3$ ,  $(\Phi_0, \mathbf{W}_0, \mathbf{H}_0) \in \mathcal{O}(M) \times F_K$

- 1:  $\Phi_J \leftarrow \text{QN}(L_S; J \times J_{\text{TL}}, \Phi_0)$
- 2:  $(\mathbf{W}_J, \mathbf{H}_J) \leftarrow \text{MU}(I_S(\Phi_J, \cdot, \cdot); J \times J_{\text{NMF}}, \mathbf{W}_0, \mathbf{H}_0)$

**Out:**  $\Phi_J, \mathbf{W}_J, \mathbf{H}_J$

---

Note that we introduced the redundant parameter  $J$  in Algorithm 2 so that the input parameters are exactly the same as for the TL-NMF solver in Algorithm 1. This allows us to ease the computational comparison of the two solvers (see Section V-E). The sub-procedures of the form  $\text{AA}(g; J, \mathbf{X})$  should be read as: executing the AA method on the function  $g$  from the initial point  $\mathbf{X}$  for  $J$  iterations.

the transform  $\Phi$ . Observing from (12) that, given  $\Phi$ , the minimization of  $C_S(\Phi, \cdot, \cdot)$  boils down to the minimization of  $I_S(\Phi, \cdot, \cdot)$ , the MU steps at line 2 of Algorithms 1 and 2 are the same and are implemented according to [30], as summarized in Algorithm 3. The latter is a block-descent algorithm in which the factors are updated in turn. The update of each factor is carried out by one step of majorization-equalization, a variant of majorization-minimization [33] that produces an acceleration while ensuring nonincreasingness of the objective function [30]. This results in the celebrated MU algorithm that is customary in NMF [9].

Concerning the update of  $\Phi$ , we adapt the quasi-Newton (QN) algorithms proposed in [34], [35]. These methods were initially developed to solve TL-NMF and JD problems with slightly different objective functions and constraints than those considered in the present work. Numerically, they have been shown to improve the convergence rate of gradient-descent or Jacobi-based methods [18], [36], [20].

#### A. General Principle of QN Methods over $\mathcal{O}(M)$

For both problems, the main difficulty in deriving a QN method for updating  $\Phi$  comes from the handling of the orthogonality constraint (i.e.,  $\Phi \in \mathcal{O}(M)$ ). In this work, we follow the standard approach that consists in defining a local parameterization  $\rho_{\Phi_j} : \Upsilon \subset \mathbb{R}^{M \times M} \rightarrow \mathcal{O}(M)$  of the neighborhood of an iterate  $\Phi_j$  (see for instance [37]). The idea is then to compute a QN direction based on a quadratic approximation of the local objective function  $g \circ \rho_{\Phi_j}$  (here  $g$  stands for either  $C_S(\cdot, \mathbf{W}, \mathbf{H})$  or  $L_S$ ). From the second-order Taylor expansion around  $\mathbf{0}$ , we get

$$g(\rho_{\Phi_j}(\mathbf{E})) = g(\Phi_j) + \langle \mathbf{G}, \mathbf{E} \rangle + \frac{1}{2} \langle \mathbf{E} | \mathcal{H} | \mathbf{E} \rangle + O(\|\mathbf{E}\|^3), \quad (36)$$

using the fact that  $\rho_{\Phi_j}(\mathbf{0}) = \Phi_j$ , and denoting respectively by  $\mathbf{G} \in \mathbb{R}^{M \times M}$  and  $\mathcal{H} \in \mathbb{R}^{M \times M \times M \times M}$  the gradient matrix and the Hessian tensor of  $g \circ \rho_{\Phi_j}$  at  $\mathbf{0}$ . In (36), the inner

**Algorithm 3** Multiplicative updates to minimize  $I_S(\Phi, \cdot, \cdot)$  [30]

**In:**  $J_{\text{NMF}} \in \mathbb{N}$ ,  $(\mathbf{W}_0, \mathbf{H}_0) \in F_K$ ,  $\mathbf{V} = \mathbb{E}_S(|\Phi \mathbf{Y}|^{\circ 2})$

- 1: **for**  $j = 0 : J_{\text{NMF}} - 1$  **do**
- 2:  $\hat{\mathbf{V}} \leftarrow \mathbf{W}_j \mathbf{H}_j + \epsilon_0 \mathbf{1}_{M \times N}$
- 3:  $\mathbf{H}_{j+1} \leftarrow \mathbf{H}_j \circ \left[ \frac{\mathbf{W}_j^\top ((\hat{\mathbf{V}})^{\circ -2} \circ \mathbf{V})}{\mathbf{W}_j^\top (\hat{\mathbf{V}})^{\circ -1}} \right]$
- 4:  $\hat{\mathbf{V}} \leftarrow \mathbf{W}_j \mathbf{H}_{j+1} + \epsilon_0 \mathbf{1}_{M \times N}$
- 5:  $\mathbf{W}_{j+1} \leftarrow \mathbf{W}_j \circ \left[ \frac{((\hat{\mathbf{V}})^{\circ -2} \circ \mathbf{V}) \mathbf{H}_{j+1}^\top}{(\hat{\mathbf{V}})^{\circ -1} \mathbf{H}_{j+1}^\top} \right]$
- 6: Normalize  $\mathbf{W}_{j+1}$ ,  $\mathbf{H}_{j+1}$  to remove scale ambiguity.
- 7: **end for**

**Out:**  $\mathbf{W}_{J_{\text{NMF}}}, \mathbf{H}_{J_{\text{NMF}}}$

**Algorithm 4** Generic quasi-Newton method to minimize a function  $g$  over  $\mathcal{O}(M)$

**In:**  $J_{\text{QN}} \in \mathbb{N}$ ,  $\Phi_0 \in \mathcal{O}(M)$ ,  $\rho_{\Phi}(\cdot)$

- 1: **for**  $j = 0 : J_{\text{QN}} - 1$  **do**
- 2: Compute the gradient  $\mathbf{G}$  and the Hessian approximation  $\tilde{\mathcal{H}}$  of the local function  $g \circ \rho_{\Phi_j}$
- 3:  $\mathbf{E}_j \leftarrow \arg \min_{\mathbf{E} \in \Upsilon} \langle \mathbf{G}, \mathbf{E} \rangle + \frac{1}{2} \langle \mathbf{E} | \tilde{\mathcal{H}} | \mathbf{E} \rangle$
- 4: Compute  $\eta > 0$  via line search
- 5:  $\Phi_{j+1} \leftarrow \rho_{\Phi_j}(\eta \mathbf{E}_j)$
- 6: **end for**

**Out:**  $\Phi_{J_{\text{TL}}}$

products should be read as  $\langle \mathbf{G}, \mathbf{E} \rangle = \sum_{a,b} [\mathbf{G}]_{ab} [\mathbf{E}]_{ab}$  and  $\langle \mathbf{E} | \tilde{\mathcal{H}} | \mathbf{E} \rangle = \sum_{a,b,c,d} [\tilde{\mathcal{H}}]_{abcd} [\mathbf{E}]_{ab} [\mathbf{E}]_{cd}$ .

Because the Hessian is usually costly to compute, we will consider an approximation of it, denoted  $\tilde{\mathcal{H}}$ , and define a QN direction through the resolution of

$$\mathbf{E}_j = \arg \min_{\mathbf{E} \in \Upsilon} \langle \mathbf{G}, \mathbf{E} \rangle + \frac{1}{2} \langle \mathbf{E} | \tilde{\mathcal{H}} | \mathbf{E} \rangle. \quad (37)$$

Given this QN direction, the current estimate  $\Phi_j$  is updated according to

$$\Phi_{j+1} = \rho_{\Phi_j}(\eta \mathbf{E}_j), \quad (38)$$

where  $\eta > 0$  is obtained by line search (e.g., backtracking [34] or Wolfe [38]). This generic QN approach is summarized in Algorithm 4. In the next two sections, we provide details on its instantiation to our problems. More precisely, the main task is to compute the gradient  $\mathbf{G}$ , the Hessian approximation  $\tilde{\mathcal{H}}$ , as well as the QN direction in (37).

**Remark 7.** In the following, we adopt two different strategies to parametrize the neighborhood of an iterate  $\Phi_j$ . The reason is that each one has been motivated independently by previous works on TL-NMF [35] and JD [34]. Yet, let us emphasize that for both problems, a QN method could be derived with each of the two local parameterizations described below.

### B. QN Method for TL-NMF

As in [35], we consider the local parameterization

$$\rho_{\Phi}(\mathbf{E}) = \exp(\mathbf{E})\Phi, \quad \forall \mathbf{E} \in \Upsilon, \quad (39)$$

where  $\Upsilon := \{\mathbf{E} \in \mathbb{R}^{M \times M} : \mathbf{E}^\top = -\mathbf{E}\}$  is the set of anti-symmetric matrices (leading to  $\exp(\mathbf{E}) \in \mathcal{O}(M)$ ). Then, denoting  $\mathbf{X}^{(s)} = \Phi \mathbf{Y}^{(s)}$ , we follow the same steps as in [35] to obtain the gradient of  $C_S(\cdot, \mathbf{W}, \mathbf{H}) \circ \rho_{\Phi}$  at  $\mathbf{0}$ ,

$$[\mathbf{G}]_{ab} = \frac{2}{S} \sum_{n,s=1}^{N,S} \frac{[\mathbf{X}^{(s)}]_{an} [\mathbf{X}^{(s)}]_{bn}}{[\mathbf{W}\mathbf{H}]_{an} + \epsilon_0}, \quad (40)$$

as well as the following diagonal Hessian approximation

$$[\tilde{\mathcal{H}}]_{abcd} = \delta_{ac} \delta_{bd} [\Gamma]_{ab} \quad (41)$$

where

$$[\Gamma]_{ab} = \frac{2}{S} \sum_{n,s=1}^{N,S} \frac{[\mathbf{X}^{(s)}]_{bn}^2}{[\mathbf{W}\mathbf{H}]_{an} + \epsilon_0}. \quad (42)$$

In Proposition 3, we provide the closed-form expression of the solution of (37) for such a diagonal  $\tilde{\mathcal{H}}$ . Again, this result is an extension of [35] to our setting (i.e., minimization of  $C_S(\cdot, \mathbf{W}, \mathbf{H})$  instead of  $I_S(\cdot, \mathbf{W}, \mathbf{H})$  in [35]).

**Proposition 3.** For  $\tilde{\mathcal{H}}$  in (41), a solution of Problem (37) is given by  $\mathbf{E} \in \Upsilon$  such that

$$[\mathbf{E}]_{ab} = \begin{cases} -\frac{[\mathbf{G}^{(\text{anti})}]_{ab}}{[\Gamma^{(\text{sym})}]_{ab}} & \text{if } [\Gamma^{(\text{sym})}]_{ab} \neq 0 \\ 0 & \text{if } [\Gamma^{(\text{sym})}]_{ab} = 0 \end{cases} \quad (43)$$

where  $\mathbf{G}^{(\text{anti})} = (\mathbf{G} - \mathbf{G}^\top)/2$  and  $\Gamma^{(\text{sym})} = (\Gamma + \Gamma^\top)/2$ . Moreover, it is a descent direction, i.e.,  $\mathbf{G}^{(\text{anti})} \neq \mathbf{0}$  implies that  $\langle \mathbf{G}, \mathbf{E} \rangle < 0$ .

*Proof.* See Appendix F-B.  $\square$

### C. QN Method for JD

For the minimization of  $L_S$ , we rely on the local parameterization discussed in [37], that is

$$\rho_{\Phi}(\mathbf{E}) = \pi(\Phi + \mathbf{E}\Phi), \quad \forall \mathbf{E} \in \Upsilon, \quad (44)$$

where  $\pi$  stands for the projection operator on  $\mathcal{O}(M)$  and  $\Upsilon$  is again the set of anti-symmetric matrices. The gradient of  $L_S \circ \rho_{\Phi}$  at  $\mathbf{0}$  is then given by

$$[\mathbf{G}]_{ab} = \frac{1}{N} \sum_{n=1}^N \left( \frac{[\Phi(\Sigma_{n,S} + \epsilon_0 \mathbf{I})\Phi^\top]_{ab}}{[\Phi(\Sigma_{n,S} + \epsilon_0 \mathbf{I})\Phi^\top]_{aa}} - \delta_{ab} \right). \quad (45)$$

Similarly to [34] (where  $L_S$  is optimized over the set of invertible matrices), we consider the Hessian approximation

$$[\tilde{\mathcal{H}}]_{abcd} = \delta_{ac} \delta_{bd} [\Gamma]_{ab} + \delta_{ad} \delta_{bc} - 2\delta_{abcd} \quad (46)$$

where

$$[\Gamma]_{ab} = \frac{1}{N} \sum_{n=1}^N \frac{[\Phi(\Sigma_{n,S} + \epsilon_0 \mathbf{I})\Phi^\top]_{bb}}{[\Phi(\Sigma_{n,S} + \epsilon_0 \mathbf{I})\Phi^\top]_{aa}}. \quad (47)$$

It is noteworthy to mention that each element of  $\mathbf{G}$  and  $\Gamma$  is well-defined as  $\forall a \leq M$ ,  $\Phi \in \mathcal{O}(M)$ ,  $[\Phi(\Sigma_{n,S} + \epsilon_0 \mathbf{I})\Phi^\top]_{aa} \geq \epsilon_0 > 0$ .

Because the Hessian approximation in (46) is not diagonal, we cannot use Proposition 3 to get the QN direction. Yet, the specific structure of  $\tilde{\mathcal{H}}$  in (46) allows to express the solution of (37) in closed form, as stated in Proposition 4.

**Proposition 4.** For  $\tilde{\mathcal{H}}$  in (46), a solution of Problem (37) is given by  $\mathbf{E} \in \Upsilon$  such that

$$[\mathbf{E}]_{ab} = \begin{cases} -\frac{[\mathbf{G}^{(\text{anti})}]_{ab}}{[\mathbf{\Gamma}^{(\text{sym})}]_{ab} - 1} & \text{if } [\mathbf{\Gamma}^{(\text{sym})}]_{ab} \neq 1 \\ 0 & \text{if } [\mathbf{\Gamma}^{(\text{sym})}]_{ab} = 1 \end{cases} \quad (48)$$

where  $\mathbf{G}^{(\text{anti})} = (\mathbf{G} - \mathbf{G}^\top)/2$  and  $\mathbf{\Gamma}^{(\text{sym})} = (\mathbf{\Gamma} + \mathbf{\Gamma}^\top)/2$ . Moreover, it is a descent direction, i.e.,  $\mathbf{G}^{(\text{anti})} \neq \mathbf{0}$  implies that  $\langle \mathbf{G}, \mathbf{E} \rangle < 0$ .

*Proof.* See Appendix F-C.  $\square$

As opposed to [34], here  $\mathbf{E}$  is constrained to be anti-symmetric. This is to ensure that, for  $\mathbf{\Phi} \in \mathcal{O}(M)$ ,  $\mathbf{E}\mathbf{\Phi}$  belongs to the tangent space of  $\mathcal{O}(M)$  at  $\mathbf{\Phi}$ . This makes  $\tilde{\mathcal{H}}$  invertible, discarding the need to rely on a pseudo-inverse.

#### D. Computational Complexity

We now briefly discuss the computational complexity of the two solvers in Algorithm 1 and 2. First of all, one can see from Algorithm 3 that an iteration of MU has a complexity of the order of  $O(KMN)$  (the main cost being the products of matrices with sizes  $M \times K$  and  $K \times N$ ).

Concerning the QN step, the main cost comes from the computation of the gradient and the Hessian approximation which lead to a complexity per iteration of the order of  $O(SNM^2)$  for TL-NMF (see (40) and (41)) and  $O(NM^3)$  for JD (see (45) and (46)).

The overall complexities of the two solvers are thus of the order of

- $O(J_{\text{NMF}}KMN + J_{\text{TL}}SNM^2)$  for TL-NMF,
- $O(J_{\text{NMF}}KMN + J_{\text{TL}}NM^3)$  for JD+NMF.

In complement of Remark 7, we see that the QN strategy deployed for TL-NMF is preferable when  $S \leq M$ , whereas the one used for JD when  $S \geq M$ . Yet, for the latter, the storage of the  $N$  covariance matrices  $\{\mathbf{\Sigma}_{n,S}\}_{n \leq N}$  is required, which results in a memory overload of  $O(NM^2)$ .

## V. NUMERICAL EXPERIMENTS

From the theoretical analysis conducted in Section III, we know that the solutions of TL-NMF and JD+NMF are getting closer as  $S$  grows. More precisely, the closeness between the solution sets of these two problems is controlled by the inner and outer  $\lambda$ 's gaps (namely  $\underline{\lambda}^\bullet - \bar{\lambda}^*$  and  $\bar{\lambda}^\bullet - \underline{\lambda}^*$ ) which converge to zero with high probability as  $S$  grows (Proposition 2 and Theorem 3). Moreover, under the GCM, they converge at least at a rate of  $O(1/S)$  (Theorem 4).

Yet, these theoretical results only provide a partial answer to the questions we identified in the introduction. For instance, the situation where  $S$  is small (including the extreme but very relevant case  $S = 1$ ) remains unclear. If TL-NMF and JD+NMF are not equivalent, does one of them provide ‘‘better’’ solutions (from an application-oriented perspective) than the other? On the other hand, when they are equivalent (i.e., when the gap is approaching zero), is one of them preferable from the point of view of computational complexity? And lastly, how tight are the derived theoretical bounds? The goal of this

section is to provide numerical insights on these questions so as to illustrate and complement our theoretical findings. The results presented in this section can be reproduced using the Python code available at <https://github.com/sixin-zh/tlnmf-tsp>.

#### A. Datasets

We consider two simulated datasets obtained respectively from a pure GCM and a blend of two synthetic music notes. The latter departs from GCM while roughly satisfying the conditions (1).

1) *GCM*: In this dataset, the dimensions are set as  $M = 10$ ,  $N = 50$ , and  $\bar{K} = 5$ . The ground-truth transform  $\bar{\mathbf{\Phi}}$  is fixed to the type-II DCT. The entries of the ground-truth NMF factors  $\bar{\mathbf{W}}$  and  $\bar{\mathbf{H}}$  are independently drawn from a Gamma distribution

$$[\bar{\mathbf{W}}]_{mk} \sim \text{Gamma}(a, \theta), \quad (49)$$

$$[\bar{\mathbf{H}}]_{kn} \sim \text{Gamma}(a, \theta), \quad (50)$$

with shape parameter  $a = 1$  and scale parameter  $\theta = 2$ . The realizations  $\{\mathbf{Y}^{(s)}\}_{s=1}^S$  are generated such that (2) holds. Note that, in the following experiments, when  $S$  is changed the  $S$  realizations are re-sampled independently using the same  $\bar{\mathbf{W}}$  and  $\bar{\mathbf{H}}$ .

2) *Synthetic Music Notes*: We follow the construction described in [5, Section III-A] which we recall for completeness. For all  $s \in \{1, \dots, S\}$ , we define the signal  $\mathbf{y}^{(s)} \in \mathbb{R}^T$  as

$$\mathbf{y}^{(s)}[t] = \sum_{i=1}^{I=2} \sum_{r=1}^{R=2} 0.5^r \cos\left(r\left(2\pi\frac{f_i}{f_0}t + \theta_i^{(s)}\right)\right) \mathbf{g}_i[t], \quad (51)$$

where  $\theta_i^{(s)} \in [0, 2\pi)$  is a uniform random phase,  $f_i > 0$  is a fundamental frequency,  $f_0 > 0$  denotes the sampling frequency,  $r$  is an integer number, and  $\mathbf{g}_i \in \mathbb{R}^T$  is a positive envelop that varies slowly over  $t \in \{1, \dots, T\}$ . In other words,  $\mathbf{y}^{(s)}$  is the sum of  $I = 2$  pure music notes with frequencies  $f_1$  and  $f_2$  that each contain  $R = 2$  harmonics. As in [5], we set the fundamental frequencies to  $f_1 = 440\text{Hz}$  (corresponding to the note A4) and  $f_2 = 466.16\text{Hz}$  (A4#), and fix  $T = 15000$  and  $f_0 = 5000\text{Hz}$ . This leads to a signal of duration 3s. The envelopes  $\mathbf{g}_1$  and  $\mathbf{g}_2$  are such that the two notes are played separately in the first two seconds and then simultaneously in the third second. Finally, the random nature of the phases  $\theta_i^{(s)}$  allows us to generate  $S$  independent signals  $\{\mathbf{y}^{(s)}\}_{s=1}^S$ .

As analyzed in [5, Section III-B], the underlying random matrix  $\mathbf{Y}$  roughly follows the conditions (1). A subset of the atoms of the ground-truth matrix  $\bar{\mathbf{\Phi}}$  captures the fundamental frequencies  $\{f_1, f_2\}$  and their harmonics  $\{2f_1, 2f_2\}$  (two orthogonal harmonic atoms per frequency to account for phase shifts). The ground-truth NMF factors  $\bar{\mathbf{W}}$  and  $\bar{\mathbf{H}}$  capture the polyphonic spectra and the activations of the two notes (hence  $\bar{K} = 2$ ).

#### B. Parameter Settings

The algorithm and model parameter values for all experiments are set to those listed in Table I. Let us comment these choices. For the GCM dataset, we set  $K = \bar{K}$ , and  $\epsilon_0 \ll \min_{m,n} [\mathbf{W}\mathbf{H}]_{mn} \simeq 1.57$ . It respects the conditions of our theoretical results in Section III. For the music notes



TABLE I  
PARAMETERS USED IN THE EXPERIMENTS:  $K$  IS THE COMMON DIMENSION OF THE NMF FACTORS ( $\mathbf{W}, \mathbf{H}$ );  $\epsilon_0$  IS DEFINED IN (4);  $J$ ,  $J_{\text{TL}}$ , AND  $J_{\text{NMF}}$  ARE THE NUMBERS OF ITERATIONS IN ALGORITHMS 1 AND 2;  $P$  DENOTES THE NUMBER OF RANDOM INITIALIZATIONS (SEE APPENDIX G).

Dataset	GCM	Music Notes
$K$	5 ( $= \bar{K}$ )	2 (see [5])
$\epsilon_0$	$10^{-8}$	$5 \times 10^{-7}$
$J_{\text{TL}}$	1	1
$J_{\text{NMF}}$	10	10
$J$	1000	100
$P$	100	10

dataset, we set  $K = 2$  to learn a NMF that can separate the two music notes. Regarding  $\epsilon_0$ , we fixed it manually, as a trade-off between numerical stability and quality of the solution in terms of recovering the fundamental frequencies of the music notes.

The number of iterations  $J_{\text{TL}}$  and  $J_{\text{NMF}}$  have been selected so as to maximize the convergence speed of TL-NMF, as they have no effect on the convergence of JD+NMF due to its two-step nature. In particular, we observed that TL-NMF enjoys a faster convergence when more NMF than TL updates are performed per outer iteration.

Finally, because they address non-convex problems, we ran the algorithms from  $P$  different initializations and we retained the best solution (in terms of objective function) for each problem. As such, we assume that we reached points that belong to (or at least are close to) the solution sets  $\Omega^*$  and  $\Omega^\bullet$ . More details on our multi-initialization strategy are provided in Appendix G.

### C. Analysis of the Gap

Next we will study the evolution of  $\hat{I}_S^\bullet$ ,  $\hat{I}_S^*$ , and  $\hat{I}_S^\bullet - \hat{I}_S^*$  as functions of the number of data realizations  $S$ . These quantities correspond to the evaluation of the function  $I_S$  at the solution points  $(\hat{\Phi}^*, \hat{\mathbf{W}}^*, \hat{\mathbf{H}}^*)$  and  $(\hat{\Phi}^\bullet, \hat{\mathbf{W}}^\bullet, \hat{\mathbf{H}}^\bullet)$  obtained through the numerical resolution of TL-NMF and JD+NMF, respectively. Given our multi-initialization strategy, we may assume that  $(\hat{\Phi}^*, \hat{\mathbf{W}}^*, \hat{\mathbf{H}}^*)$  and  $(\hat{\Phi}^\bullet, \hat{\mathbf{W}}^\bullet, \hat{\mathbf{H}}^\bullet)$  belong to (or at least are close to) the solution sets  $\Omega^*$  and  $\Omega^\bullet$ . Note that from Theorem 2, Proposition 2, and by construction of  $\hat{I}_S^*$  and  $\hat{I}_S^\bullet$ , we expect the following inequalities

$$\underline{\lambda}^* \leq \hat{I}_S^* \leq \bar{\lambda}^* \leq \underline{\lambda}^\bullet \leq \hat{I}_S^\bullet \leq \bar{\lambda}^\bullet \leq \max_{\Phi \in \mathcal{O}(M)} Q_S(\Phi). \quad (52)$$

Figure 2 displays the values of  $\hat{I}_S^\bullet$ ,  $\hat{I}_S^*$ , and  $\hat{I}_S^\bullet - \hat{I}_S^*$  for the GCM and music notes datasets. For the GCM dataset, we observe that  $\hat{I}_S^*$  decays as  $O(1/S)$  which implies that all the quantities in (52) (except  $\underline{\lambda}^*$ ) enjoy at best the same rate of convergence. In particular, this constitutes an additional evidence that the bound derived in Remark 5 is tight (also complementing Remark 6). It further shows that the bound in Proposition 2 is also tight (under GCM). Concerning the gap

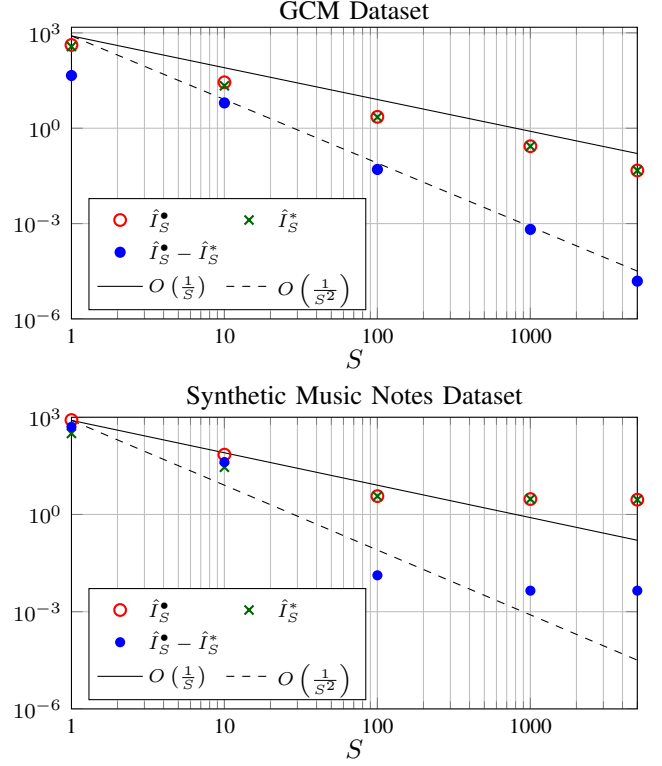


Fig. 2. Evolution of the empirical quantities  $\hat{I}_S^\bullet$ ,  $\hat{I}_S^*$ , and  $\hat{I}_S^\bullet - \hat{I}_S^*$  as functions of the number of realizations  $S$ .

$\hat{I}_S^\bullet - \hat{I}_S^*$ , we observe in Figure 2 that it converges at the faster rate of  $O(1/S^2)$ . From (25) and (27), this implies that the convergence rate of the inner gap  $\bar{\lambda}^\bullet - \bar{\lambda}^*$  is at least of the order of  $O(1/S^2)$  while the outer gap  $\bar{\lambda}^\bullet - \underline{\lambda}^*$  converges at a rate that lies between  $O(1/S^2)$  and  $O(1/S)$ . We can draw two possible hypothesis from this. The first one is that both gaps would enjoy the same rate of convergence of  $O(1/S^2)$  which would mean that our upper bound in (27) is loose (as we have seen that bounds in Proposition 2 and Theorem 4 are tight). A direct analysis of  $\bar{\lambda}^\bullet - \underline{\lambda}^*$  rather than  $\bar{\lambda}^\bullet$  would thus be of interest. The second possible interpretation is that the two gaps would indeed not converge at the same rate and thus that a finer analysis would require to consider both gaps separately.

Concerning the music notes dataset, we observe that all the reported quantities are decaying up to  $S \leq 100$ . However, as  $S$  further grows, the quantity  $\hat{I}_S^\bullet$  seems to tend toward a constant.

Although a theoretical explanation of this phenomenon remains an open problem, it is likely due to the fact that the data do not exactly follow the conditions (1). Nevertheless, the solutions returned by TL-NMF and JD+NMF on this dataset remain very close when  $S$  is large, as illustrated next.

### D. Analysis of the Solutions

In Figure 3, we display the solutions obtained by TL-NMF and JD+NMF on the music notes dataset for both  $S = 1$  and  $S = 100$ . As expected, when  $S$  is large both approaches are able to learn a transform  $\Phi$  that captures the exact fundamental

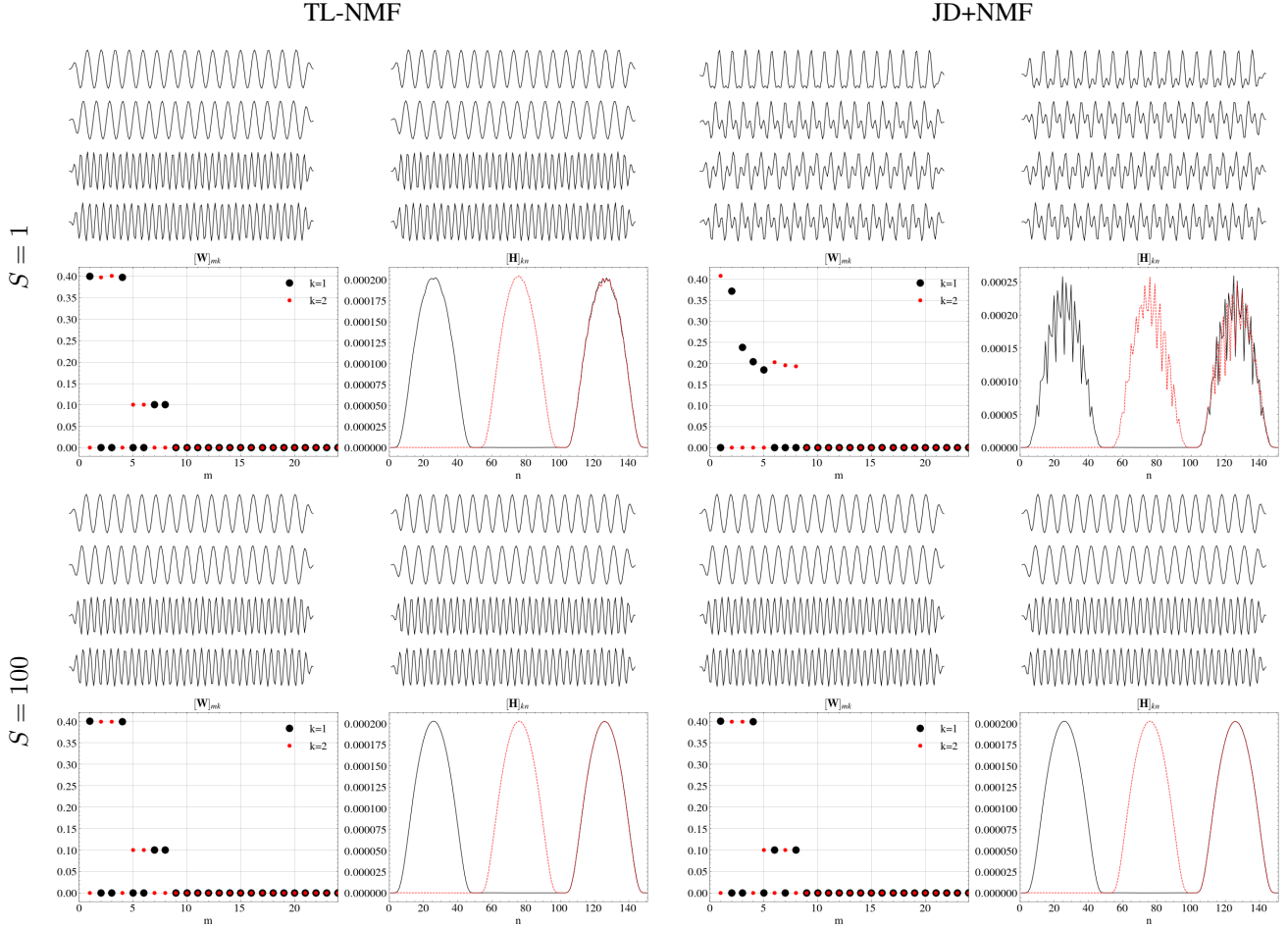


Fig. 3. Plots of the eight most significant atoms (rows) of the learnt  $\Phi$  as well as the two columns of the estimated  $\mathbf{W}$  and two rows of the estimated  $\mathbf{H}$  for the music notes dataset. The most significant atoms are chosen as those that maximize  $\mathbb{E}_S \|\underline{\phi}_k \mathbf{Y}\|_2^2$ , where  $\underline{\phi}_k$  is the  $k^{\text{th}}$  row of  $\Phi$ .

and harmonic frequencies of the two musical notes, allowing to significantly surpass the source separation performance of standard NMF that must abide to arbitrary frequency grid of the chosen DCT or Fourier frequency transform (see [5]).

However, the picture is quite different for  $S = 1$ . Although the solution provided by TL-NMF appears to be as good as for  $S = 100$  (i.e., it enjoys the same favorable properties), the solution of JD+NMF is visibly degraded. To further quantify the differences between the atoms learnt by TL-NMF and JD+NMF, we performed a nonlinear least-square regression of the learnt atoms with the harmonic model  $(a, f, \theta) \mapsto a \cos(2\pi \frac{f}{f_0} \cdot + \theta)$ , as in [5]. We report in Table II the estimated frequency  $f$  for an atom  $\underline{\phi} \in \mathbb{R}^M$ , together with the regression error  $\|\underline{\phi} - a \cos(2\pi \frac{f}{f_0} \cdot + \theta)\|^2$ . We observe that the eight most significant atoms of TL-NMF ( $S = 1$ ) lead to a better fit to the fundamental frequencies of the two music notes due to smaller regression errors. These errors could also explain why the NMF factors  $\mathbf{W}^\bullet$  and  $\mathbf{H}^\bullet$  are less regular in JD+NMF. These observations are in line with Figure 2 where we see that, when  $S$  is small, the numerical gap  $\hat{I}_S^\bullet - \hat{I}_S^*$  is quite large, meaning that the transform  $\Phi^*$  learnt by TL-NMF performs better in making  $\mathbb{E}_S([\Phi \mathbf{Y}]_{mn}^2)$  more amenable to a low-rank NMF approximation than the transform  $\Phi^\bullet$  obtained by JD+NMF.

TABLE II  
FREQUENCIES AND REGRESSION ERRORS OF THE TL-NMF AND JD+NMF ATOMS WHEN  $S = 1$  (SAME ORDER AS IN FIG. 3).

TL-NMF		JD+NMF	
Freq.	Error	Freq.	Error
440.10	0.03	466.12	0.19
466.35	0.03	439.72	0.37
466.11	0.04	879.97	0.51
439.74	0.04	879.99	0.45
932.32	0.03	879.97	0.44
932.39	0.04	932.46	0.42
879.94	0.04	932.28	0.40
879.99	0.03	932.31	0.39

### E. Computational Complexity

When JD+NMF provides solutions that are very close to those of TL-NMF (i.e., when  $S$  is large), it is of interest to compare the computational load of the two methods. To that end, we fix  $J_{\text{TL}} = 1$ ,  $J_{\text{NMF}} = 10$  and compute, for several values  $J \in \mathbb{N}$ ,

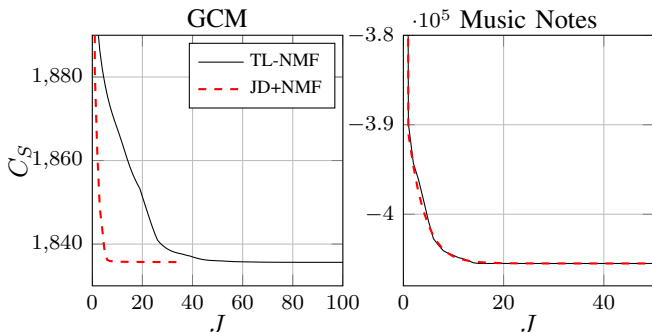


Fig. 4. Evolution of  $C_S$  (for  $S = 100$ ) as a function of the parameter  $J$  in Algorithms 1 and 2.

- $(\Phi_J^*, \mathbf{W}_J^*, \mathbf{H}_J^*)$ : the solution obtained after  $J$  iterations of TL-NMF (each composed of  $J_{\text{TL}}$  updates of  $\Phi$  and  $J_{\text{NMF}}$  updates of  $(\mathbf{W}, \mathbf{H})$ ),
- $(\Phi_J^\bullet, \mathbf{W}_J^\bullet, \mathbf{H}_J^\bullet)$ : the solution obtained after  $(J \times J_{\text{TL}})$  iterations of JD and  $(J \times J_{\text{NMF}})$  NMF updates.

By doing so, given  $J \in \mathbb{N}$ , the number of cumulative updates of  $\Phi$  and  $(\mathbf{W}, \mathbf{H})$  for both methods is the same and the comparison is fair.

We report in Figure 4 the evolution of  $C_S(\Phi_J^*, \mathbf{W}_J^*, \mathbf{H}_J^*)$  and  $C_S(\Phi_J^\bullet, \mathbf{W}_J^\bullet, \mathbf{H}_J^\bullet)$  as a function of  $J$  for  $S = 100$ . While on the music notes dataset both methods converge at a similar speed, we can see that JD+NMF converges faster than TL-NMF on the GCM dataset. This suggests that, in the situation where JD+NMF meets TL-NMF, the former should be preferred from the perspective of the computational complexity.

## VI. DISCUSSION AND CONCLUDING REMARKS

From our theoretical and numerical analysis, we can describe the relationship between TL-NMF and JD+NMF by distinguishing two situations. On the one hand, when  $S$  is large and  $K \geq \bar{K}$ , the two problems are equivalent (Theorems 2 and 3) and—at least on the reported numerical experiments—JD+NMF seems to enjoy a faster convergence (Figure 4). On the other hand, when  $S$  is small (in particular  $S = 1$ ), they are not equivalent anymore and the solutions obtained by TL-NMF appear to be more meaningful from an application point of view (Figure 3). One explanation of this phenomenon comes from the inherent low-rank constraint in the  $\Phi$  update of TL-NMF which favors the learning of orthogonal transforms that are better suited to a low-rank NMF. This is clearly visible when comparing the values of  $I_S$  at the obtained solutions (see Figure 2 and Theorem 2).

In this work, we fixed  $\mathbb{E}_S(|\Phi \mathbf{Y}|^2)$  to the empirical expectation given by (10), which naturally led us to analyze the relationship between the two problems as a function of the number of realizations  $S$ . However, we can see from Proposition 2 that the main ingredient to make TL-NMF and JD+NMF equivalent is to build a good estimator of the variance  $\mathbb{E}(|\Phi \mathbf{Y}|^2)$ , in the sense that the Itakura-Saito divergence between the estimator and the true expectation is small (i.e.,  $Q_S(\Phi)$  uniformly small). The empirical expectation is a natural choice when

several signal realizations are available, but other choices are possible. Indeed, even for  $S = 1$ , the variance  $\mathbb{E}(|\Phi \mathbf{Y}|^2)$  can be estimated by a local moving average, under suitable local stationary assumptions. An example is when  $\mathbf{H}$  is given a block structure (with identical columns inside the blocks), similarly to the *block Gaussian model* of [14]. Actually, such a block structure can be seen alternatively as having access to several realizations of  $\mathbf{Y}$  (with  $S > 1$  the size of the block).

In this paper we only considered real-valued transform for mathematical convenience. Complex-valued transform such as the short-time Fourier transform (STFT) are more customary in audio signal processing (in particular for shift-invariance). Extending our work to such complex-valued transform is an appealing research direction. Note also that the complex-valued Fourier transform is an orthogonal transform endowed with a specific form of Hermitian symmetry. In particular, when applied to real-valued signals, only half of the power spectrum needs to be considered. Imposing such a structure to  $\Phi$ , to mimic some of the properties of the Fourier transform, would be a very interesting topic. This is however a challenging problem, both in terms of mathematical analysis and design of optimisation methods. Another exciting research direction would be to lift the orthogonal constraint imposed on  $\Phi$  and only assume invertibility. However, for TL-NMF to be useful to signal processing tasks, it is important that  $\Phi$  can be inverted for temporal reconstruction and thus that its inverse be well-conditioned. Existing JD algorithms such that [24], [25] might be useful for this purpose.

## APPENDIX A PROOF OF LEMMA 1

The objective  $L_S$  in (13) can be rewritten as

$$L_S(\Phi) = MN + \sum_{n=1}^N \log \left( \prod_{m=1}^M (\mathbb{E}_S([\Phi \mathbf{Y}]_{mn}^2) + \epsilon_0) \right) \quad (53)$$

Then from the definition of the empirical expectation in (10) and the orthogonality of  $\Phi$ , we have that for every  $(m, n)$ ,

$$\begin{aligned} \mathbb{E}_S([\Phi \mathbf{Y}]_{mn}^2) + \epsilon_0 &= \left[ \frac{1}{S} \sum_{s=1}^S (\Phi \mathbf{y}_n^{(s)}) (\Phi \mathbf{y}_n^{(s)})^\top + \epsilon_0 \mathbf{I} \right]_{mm} \\ &\stackrel{(11)}{=} [\Phi (\Sigma_{n,S} + \epsilon_0 \mathbf{I}) \Phi^\top]_{mm}. \end{aligned} \quad (54)$$

Therefore combining the formula (54) with (53), we have

$$L_S(\Phi) = MN + \sum_{n=1}^N \log \det \text{Diag} (\Phi (\Sigma_{n,S} + \epsilon_0 \mathbf{I}) \Phi^\top).$$

Finally, the JD criterion derived in [14], that is

$$\begin{aligned} \sum_{n=1}^N \log \det \text{Diag} (\Phi (\Sigma_{n,S} + \epsilon_0 \mathbf{I}) \Phi^\top) - \\ \log \det (\Phi ((\Sigma_{n,S} + \epsilon_0 \mathbf{I}) \Phi^\top)), \end{aligned} \quad (55)$$

equals  $L_S$  up to a constant term because, for  $\Phi$  orthogonal,  $\det(\Phi (\Sigma_{n,S} + \epsilon_0 \mathbf{I}) \Phi^\top) = \det(\Sigma_{n,S} + \epsilon_0 \mathbf{I})$ .

APPENDIX B  
PROOF OF THEOREM 1

A. Existence of a Solution for JD+NMF (Problem (6))

Given the two-step nature of Problem (6), the existence of a solution  $(\Phi^\bullet, \mathbf{W}^\bullet, \mathbf{H}^\bullet) \in \Omega^\bullet$  is a direct consequence of the following two lemmas.

**Lemma 2.** *The set of global minimizers of  $L_S$  over  $\mathcal{O}(M)$  is nonempty and compact.*

*Proof.* As  $\epsilon_0 > 0$ ,  $\log(\mathbb{E}_S([\Phi\mathbf{Y}]_{mn}^2) + \epsilon_0)$  is well defined and  $L_S$  is continuous on the compact manifold  $\mathcal{O}(M)$ . Therefore  $\inf_{\Phi \in \mathcal{O}(M)} L_S(\Phi)$  is attained and finite (Weierstrass Theorem). Furthermore, the solution set is closed (it is a level set of the continuous function  $L_S$ ) and bounded because it is included in the bounded set  $\mathcal{O}(M)$ . This proves the compactness and completes the proof.  $\square$

**Lemma 3.** *For all  $\Phi \in \mathcal{O}(M)$ , the set of global minimizers of  $I_S(\Phi, \cdot, \cdot)$  over  $F_K$  is nonempty and compact.*

*Proof.* By definition, for all  $\Phi \in \mathcal{O}(M)$ ,  $I_S(\Phi, \cdot, \cdot)$  is continuous over  $F_K$ . As  $F_K$  is closed but unbounded, a sufficient argument to complete the proof is to show that, for all  $\Phi \in \mathcal{O}(M)$ ,  $I_S(\Phi, \cdot, \cdot)$  is coercive over  $F_K$ , i.e.,

$$\forall \Phi \in \mathcal{O}(M), \lim_{\substack{\|(\mathbf{W}, \mathbf{H})\|_{1,1} \rightarrow \infty \\ (\mathbf{W}, \mathbf{H}) \in F_K}} I_S(\Phi, \mathbf{W}, \mathbf{H}) = +\infty. \quad (56)$$

Since all norms being equivalent in finite dimension, we use the norm  $\|(\mathbf{W}, \mathbf{H})\|_{1,1} = \|\mathbf{W}\|_{1,1} + \|\mathbf{H}\|_{1,1}$ , where  $\|\cdot\|_{1,1}$  denotes the entrywise  $\ell_1$ -norm for matrices. Because of the normalization constraint on  $\mathbf{W}$  in  $F_K$ , we have

$$\forall (\mathbf{W}, \mathbf{H}) \in F_K, \|(\mathbf{W}, \mathbf{H})\|_{1,1} = K + \|\mathbf{H}\|_{1,1}. \quad (57)$$

Now, let  $\Phi \in \mathcal{O}(M)$ ,  $\nu > 0$  and set

$$\rho = KMNe^{\nu + \log(D)+1} + K > K, \quad (58)$$

where  $D = \max_{m,n} \mathbb{E}_S([\Phi\mathbf{Y}]_{m,n}^2) + \epsilon_0 > 0$ . Then we have the following implications:

$$\begin{aligned} (\mathbf{W}, \mathbf{H}) \in F_K \text{ and } \|(\mathbf{W}, \mathbf{H})\|_{1,1} \geq \rho \\ \implies \|\mathbf{H}\|_{1,1} \geq \rho - K > 0 \\ \implies \exists (k_0, n_0) \text{ s.t. } h_{k_0 n_0} \geq \frac{\rho - K}{KN}, \end{aligned} \quad (59)$$

where the last implication comes from the fact that  $\mathbf{H} \in \mathbb{R}_+^{K \times N}$ . Similarly, using the fact that  $\mathbf{w}_{k_0} \in \mathbb{R}_+^M$  and  $\|\mathbf{w}_{k_0}\|_1 = 1$ , we get that  $\exists m_0$  s.t.  $w_{m_0 k_0} \geq 1/M$ . Combining the latter with (59), we obtain

$$[\mathbf{W}\mathbf{H}]_{m_0 n_0} \geq \frac{\rho - K}{MKN} \stackrel{(58)}{\geq} e^{\nu + \log(D)+1}. \quad (60)$$

Finally, denoting  $f(x) = x - \log(x) - 1$  we have

$$\begin{aligned} I_S(\Phi, \mathbf{W}, \mathbf{H}) &= \sum_{m,n=1}^{M,N} f\left(\frac{\mathbb{E}_S([\Phi\mathbf{Y}]_{mn}^2) + \epsilon_0}{[\mathbf{W}\mathbf{H}]_{mn} + \epsilon_0}\right) \\ &\geq f\left(\frac{\mathbb{E}_S([\Phi\mathbf{Y}]_{m_0 n_0}^2) + \epsilon_0}{[\mathbf{W}\mathbf{H}]_{m_0 n_0} + \epsilon_0}\right) \quad (\text{as } f \geq 0 \text{ on } \mathbb{R}_+) \\ &\geq -\log\left(\frac{\mathbb{E}_S([\Phi\mathbf{Y}]_{m_0 n_0}^2) + \epsilon_0}{[\mathbf{W}\mathbf{H}]_{m_0 n_0} + \epsilon_0}\right) - 1 \\ &\geq \log([\mathbf{W}\mathbf{H}]_{m_0 n_0} + \epsilon_0) - \log(D) - 1 \stackrel{(60)}{\geq} \nu. \end{aligned}$$

Hence, we have shown that for all  $\Phi \in \mathcal{O}(M)$  and all  $\nu > 0$ , there exists  $\rho > 0$  (i.e., (58)) such that

$$\begin{aligned} (\mathbf{W}, \mathbf{H}) \in F_K \text{ and } \|(\mathbf{W}, \mathbf{H})\|_{1,1} \geq \rho \\ \implies I_S(\Phi, \mathbf{W}, \mathbf{H}) \geq \nu, \end{aligned} \quad (61)$$

which completes the proof.  $\square$

B. Existence of a Solution for the TL-NMF Problem (3)

From Lemma 3, we get that the function

$$O_S(\Phi) = \min_{(\mathbf{W}, \mathbf{H}) \in F_K} I_S(\Phi, \mathbf{W}, \mathbf{H}), \quad (62)$$

is well defined on  $\mathcal{O}(M)$  in the sense that the min exists for any  $\Phi \in \mathcal{O}(M)$ . As such, from the decomposition of  $C_S$  in (12) and given that  $\mathcal{O}(M)$  is compact and  $L_S$  continuous, it is sufficient to prove that  $O_S$  is continuous over  $\mathcal{O}(M)$  (done by Lemma 4) and invoke the Weierstrass Theorem to complete the proof that  $\Omega^*$  is non-empty.

**Lemma 4.** *The function  $O_S$  defined in (62) is continuous over  $\mathcal{O}(M)$ .*

*Proof.* We need to show that, for any  $\Phi \in \mathcal{O}(M)$  and  $\mathbf{D} \in \mathcal{T}_\Phi$  (the tangent space of  $\mathcal{O}(M)$  at  $\Phi$ ),

$$\lim_{\delta \rightarrow 0} |O_S(\pi(\Phi + \delta\mathbf{D})) - O_S(\Phi)| = 0, \quad (63)$$

where  $\pi$  stands for the projection operator on  $\mathcal{O}(M)$  [37].

Let  $\Phi \in \mathcal{O}(M)$ ,  $\mathbf{D} \in \mathcal{T}_\Phi$  and  $(\mathbf{W}_\delta, \mathbf{H}_\delta) \in F_K$  be a global minimizer of  $I_S(\pi(\Phi + \delta\mathbf{D}), \cdot, \cdot)$  (there exists at least one from Lemma 3). Then,

$$O_S(\pi(\Phi + \delta\mathbf{D})) - O_S(\Phi) \leq g_\delta(\mathbf{W}_0, \mathbf{H}_0) \quad (64)$$

$$O_S(\pi(\Phi + \delta\mathbf{D})) - O_S(\Phi) \geq g_\delta(\mathbf{W}_\delta, \mathbf{H}_\delta), \quad (65)$$

with  $g_\delta(\mathbf{W}, \mathbf{H}) = I_S(\pi(\Phi + \delta\mathbf{D}), \mathbf{W}, \mathbf{H}) - I_S(\Phi, \mathbf{W}, \mathbf{H})$ . Moreover, from the definition of  $I_S$  in (14)–(15), we get that for all  $(\mathbf{W}, \mathbf{H}) \in F_K$ ,

$$\begin{aligned} |g_\delta(\mathbf{W}, \mathbf{H})| &\leq \sum_{m,n=1}^{M,N} \left| \log\left(\frac{\mathbb{E}_S[\pi(\Phi + \delta\mathbf{D})\mathbf{Y}]_{mn}^2 + \epsilon_0}{\mathbb{E}_S[\Phi\mathbf{Y}]_{mn}^2 + \epsilon_0}\right) \right| \\ &\quad + \frac{1}{\epsilon_0} |\mathbb{E}_S([\pi(\Phi + \delta\mathbf{D})\mathbf{Y}]_{mn}^2) - \mathbb{E}_S([\Phi\mathbf{Y}]_{mn}^2)|. \end{aligned} \quad (66)$$

Because the right-hand side is independent of  $(\mathbf{W}, \mathbf{H})$  and converges to 0 as  $\delta$  tends to 0, we obtain

$$\lim_{\delta \rightarrow 0} |g_\delta(\mathbf{W}_0, \mathbf{H}_0)| = 0, \quad \lim_{\delta \rightarrow 0} |g_\delta(\mathbf{W}_\delta, \mathbf{H}_\delta)| = 0. \quad (67)$$

Finally, combining (67) with (64)–(65) proves (63).  $\square$

### C. Compactness of $\Omega^\bullet$

Given that  $\Omega^\bullet$  is finite dimensional, it is sufficient to show, according to Heine–Borel theorem, that it is a non-empty (already proved), closed, and bounded set.

1) *Closedness*: Let  $\{(\Phi_j, \mathbf{W}_j, \mathbf{H}_j) \in \Omega^\bullet\}_j$  be a sequence of  $\Omega^\bullet$  that converges toward  $(\widehat{\Phi}, \widehat{\mathbf{W}}, \widehat{\mathbf{H}})$ . Then, from the continuity of  $I_S$  and the fact that (by definition of  $\Omega^\bullet$ ),

$$I_S(\Phi_j, \mathbf{W}_j, \mathbf{H}_j) \leq I_S(\widehat{\Phi}, \mathbf{W}, \mathbf{H}), \quad \forall (\mathbf{W}, \mathbf{H}) \in F_K, \quad (68)$$

we obtain

$$I_S(\widehat{\Phi}, \widehat{\mathbf{W}}, \widehat{\mathbf{H}}) \leq I_S(\widehat{\Phi}, \mathbf{W}, \mathbf{H}), \quad \forall (\mathbf{W}, \mathbf{H}) \in F_K. \quad (69)$$

Noticing that  $\widehat{\Phi} \in \arg \min_{\Phi \in \mathcal{O}(M)} L_S(\Phi)$  (compactness of the set of minimizers of  $L_S$ , Lemma 2), we conclude from (69) that  $(\widehat{\Phi}, \widehat{\mathbf{W}}, \widehat{\mathbf{H}}) \in \Omega^\bullet$ , which shows that  $\Omega^\bullet$  is closed.

2) *Boundedness*: Let us assume that  $\Omega^\bullet$  is unbounded. Hence, there exists a sequence  $\{(\Phi_j, \mathbf{W}_j, \mathbf{H}_j) \in \Omega^\bullet\}_j$  such that

$$\lim_{j \rightarrow \infty} \|(\Phi_j, \mathbf{W}_j, \mathbf{H}_j)\|_{1,1} = +\infty. \quad (70)$$

Then, using the fact that  $\mathcal{O}(M)$  is compact, we get that the norm of  $\Phi_j$  is bounded and thus, with (57) and (70), that  $\lim_{j \rightarrow \infty} \|\mathbf{H}_j\|_{1,1} = +\infty$ . It follows from the coercivity of  $I_S$  (see Lemma 3) that

$$\lim_{j \rightarrow \infty} O_S(\Phi_j) = \lim_{(62) j \rightarrow \infty} I_S(\Phi_j, \mathbf{W}_j, \mathbf{H}_j) = +\infty, \quad (71)$$

which contradicts the fact that  $O_S$  is a continuous function over the compact set  $\mathcal{O}(M)$  (see Lemma 4).

### D. Compactness of $\Omega^*$

Again, because  $\Omega^*$  is finite dimensional, it is sufficient to show that  $\Omega^*$  is a non-empty (already proved), closed, and bounded set. Here, we directly get that  $\Omega^*$  is closed as a level set of the continuous function  $C_S$ . Then, let us assume that  $\Omega^*$  is unbounded. Hence, using the same arguments as in the proof for  $\Omega^\bullet$ , this means that there exists a sequence  $\{(\Phi_j, \mathbf{W}_j, \mathbf{H}_j) \in \Omega^*\}_j$  for which  $\lim_{j \rightarrow \infty} \|\mathbf{H}_j\|_{1,1} = +\infty$ . Hence, because

$$C_S(\Phi_j, \mathbf{W}_j, \mathbf{H}_j) \geq \sum_{m,n=1}^{M,N} \log([\mathbf{W}_j \mathbf{H}_j]_{mn} + \epsilon_0), \quad (72)$$

we have

$$\lim_{j \rightarrow \infty} C_S(\Phi_j, \mathbf{W}_j, \mathbf{H}_j) = +\infty, \quad (73)$$

which contradicts the fact that  $\forall j, (\Phi_j, \mathbf{W}_j, \mathbf{H}_j) \in \Omega^*$ .

## APPENDIX C PROOF OF THEOREM 2

First of all, the continuity of  $I_S$  together with the compactness of  $\Omega^*$  and  $\Omega^\bullet$  ensures the existence of the max and min in (17)–(18) (Weierstrass Theorem). The following three proofs rely on the key Equation (12) which states that  $C_S = L_S + I_S$ .

*Proof of (19)*: By definition, we have  $\underline{\lambda}^* \leq \bar{\lambda}^*$  and  $\underline{\lambda}^* \leq \bar{\lambda}^*$ . Moreover, the lower bound 0 in (19) is due to the fact that  $I_S \geq 0$ . It thus remains to show that  $\bar{\lambda}^* \leq \underline{\lambda}^*$ . Let us assume that  $\bar{\lambda}^* > \underline{\lambda}^*$ . Hence there exist  $(\Phi^*, \mathbf{W}^*, \mathbf{H}^*) \in \Omega^*$  and  $(\Phi^\bullet, \mathbf{W}^\bullet, \mathbf{H}^\bullet) \in \Omega^\bullet$  such that

$$I_S(\Phi^*, \mathbf{W}^*, \mathbf{H}^*) > I_S(\Phi^\bullet, \mathbf{W}^\bullet, \mathbf{H}^\bullet) \quad (74)$$

$$\stackrel{(12)}{\iff} C_S(\Phi^*, \mathbf{W}^*, \mathbf{H}^*) > L_S(\Phi^*) + I_S(\Phi^\bullet, \mathbf{W}^\bullet, \mathbf{H}^\bullet) \quad (75)$$

$$\implies C_S(\Phi^*, \mathbf{W}^*, \mathbf{H}^*) > C_S(\Phi^\bullet, \mathbf{W}^\bullet, \mathbf{H}^\bullet), \quad (76)$$

where the last implication comes from the fact that  $L_S(\Phi^*) \geq L_S(\Phi^\bullet)$ . This contradicts the fact that  $(\Phi^*, \mathbf{W}^*, \mathbf{H}^*)$  is a global minimizer of  $C_S$  and completes the proof of (19).

*Proof of (20) and (21)*: The inclusion  $\implies$  is straightforward from (19) together with the definition of  $\bar{\lambda}^*$  and  $\underline{\lambda}^*$ . Now, if  $\bar{\lambda}^* = \underline{\lambda}^*$ , then there exist  $(\Phi^*, \mathbf{W}^*, \mathbf{H}^*) \in \Omega^*$  and  $(\Phi^\bullet, \mathbf{W}^\bullet, \mathbf{H}^\bullet) \in \Omega^\bullet$  such that

$$I_S(\Phi^*, \mathbf{W}^*, \mathbf{H}^*) = I_S(\Phi^\bullet, \mathbf{W}^\bullet, \mathbf{H}^\bullet) \quad (77)$$

$$\stackrel{(12)}{\iff} C_S(\Phi^*, \mathbf{W}^*, \mathbf{H}^*) = L_S(\Phi^*) + I_S(\Phi^\bullet, \mathbf{W}^\bullet, \mathbf{H}^\bullet) \quad (78)$$

$$\implies C_S(\Phi^*, \mathbf{W}^*, \mathbf{H}^*) \geq C_S(\Phi^\bullet, \mathbf{W}^\bullet, \mathbf{H}^\bullet). \quad (79)$$

Given that  $(\Phi^*, \mathbf{W}^*, \mathbf{H}^*)$  is a global minimizer of  $C_S$ , we have  $C_S(\Phi^*, \mathbf{W}^*, \mathbf{H}^*) = C_S(\Phi^\bullet, \mathbf{W}^\bullet, \mathbf{H}^\bullet)$ . Moreover, the latter equality with (77) lead to  $L_S(\Phi^*) = L_S(\Phi^\bullet)$ . This completes the proof.

*Proof of (21)*: can be obtained following the same steps.

## APPENDIX D PROOF OF PROPOSITION 2

First of all, one can easily see that

$$\bar{\lambda}^* \leq \max_{\Phi \in \mathcal{O}(M)} O_S(\Phi), \quad (80)$$

where  $O_S$  is defined as in (62). To complete the proof, we shall show that,  $\forall \Phi \in \mathcal{O}(M)$ ,  $O_S(\Phi) \leq Q_S(\Phi)$  where  $Q_S$  is defined in (29).

To that end, let us show<sup>2</sup> that, for any  $\Phi \in \mathcal{O}(M)$ , there exist  $(\mathbf{W}_\Phi^*, \mathbf{H}_\Phi^*) \in F_K$  such that  $\mathbb{E}([\Phi \mathbf{Y}]_{mn}^2) = \mathbf{W}_\Phi^* \mathbf{H}_\Phi^*$ . Let  $\mathbf{D} = \Phi \Phi^\top$ ,  $\bar{\mathbf{V}} = \bar{\mathbf{W}} \bar{\mathbf{H}}$  with  $\bar{v}_{mn} = [\bar{\mathbf{V}}]_{mn}$  and  $d_{mm'} = [\mathbf{D}]_{mm'}$ . Then, from (7) and (8) we have

$$\mathbb{E}([\Phi \mathbf{Y}]_{mn}^2) = \mathbb{E} \left( \left( \sum_{m'=1}^M d_{mm'} [\bar{\Phi} \mathbf{Y}]_{m'n} \right)^2 \right) \quad (81)$$

$$= \sum_{m'=1}^M d_{mm'}^2 \bar{v}_{m'n} \quad (82)$$

$$= \sum_{k=1}^{\bar{K}} \sum_{m'=1}^M d_{mm'}^2 \bar{w}_{m'k} \bar{h}_{kn} \quad (83)$$

For (81), we used the orthogonality of  $\bar{\Phi}$  to get  $\Phi = \mathbf{D} \bar{\Phi}$ . Defining  $(\mathbf{W}_\Phi^*, \mathbf{H}_\Phi^*) \in \mathbb{R}_+^{M \times K} \times \mathbb{R}_+^{K \times N}$  such that

$$[\mathbf{W}_\Phi^*]_{mk} = \begin{cases} \sum_{m'} \frac{\bar{w}_{m'k}}{\|\bar{\mathbf{w}}_k\|} d_{mm'}^2 & \text{if } k \leq \bar{K}, \\ \frac{1}{M} & \text{if } \bar{K} < k \leq K, \end{cases} \quad (84)$$

<sup>2</sup>This result was already shown in [5] without the constraint set  $F_K$ . For completeness, we recall all the steps here.

$$[\mathbf{H}_\Phi^*]_{kn} = \begin{cases} \bar{h}_{kn} \|\bar{\mathbf{w}}_k\|_1 & \text{if } k \leq \bar{K}, \\ 0 & \text{if } \bar{K} < k \leq K, \end{cases} \quad (85)$$

we get from (83) that

$$\mathbf{W}_\Phi^* \mathbf{H}_\Phi^* = \mathbb{E}(|\Phi \mathbf{Y}|^{\circ 2}). \quad (86)$$

Moreover, as  $\sum_m d_{mm'}^2 = 1$ , we obtain that, for all  $k \leq \bar{K}$ ,

$$\sum_{m=1}^M [\mathbf{W}_\Phi^*]_{mk} = \sum_{m'=1}^M \frac{\bar{w}_{m'k}}{\|\bar{\mathbf{w}}_k\|_1} \sum_{m=1}^M d_{mm'}^2 = 1. \quad (87)$$

Given that, by definition in (84), we also have  $\sum_{m=1}^M [\mathbf{W}_\Phi^*]_{mk} = 1$  for  $\bar{K} < k \leq K$ . Therefore we have shown that  $(\mathbf{W}_\Phi^*, \mathbf{H}_\Phi^*) \in F_K$ .

It follows from (86) that,  $\forall \Phi \in \mathcal{O}(M)$ ,

$$O_S(\Phi) \leq I_S(\Phi, \mathbf{W}_\Phi^*, \mathbf{H}_\Phi^*) \quad (88)$$

$$= D_{\epsilon_0}(\mathbb{E}_S(|\Phi \mathbf{Y}|^{\circ 2}) | \mathbf{W}_\Phi^* \mathbf{H}_\Phi^*) = Q_S(\Phi). \quad (89)$$

#### APPENDIX E PROOF OF THEOREMS 3 AND 4

##### A. Preliminaries

In Lemma 5 we derive an equivalent formulation of condition (30) that is more convenient to prove Theorems 3 and 4.

**Lemma 5.** *Condition (30) is satisfied if and only if  $U_S \xrightarrow{p} 0$  as  $S \rightarrow \infty$  where*

$$U_S = \max_{m,n} \max_{\Phi \in \mathcal{O}(M)} \left| \frac{\mathbb{E}_S([\Phi \mathbf{Y}]_{mn}^2) + \epsilon_0}{\mathbb{E}([\Phi \mathbf{Y}]_{mn}^2) + \epsilon_0} - 1 \right| \quad (90)$$

$$\leq \max_n \|\Sigma_n^{-1/2} \Sigma_{n,S} \Sigma_n^{-1/2} - \mathbf{I}\|. \quad (91)$$

*Proof.* Given the fact that  $[\bar{\mathbf{W}}\bar{\mathbf{H}}]_{mn} > 0 \forall (m, n)$ , we introduce two constants  $\epsilon_1 > 0$  and  $\epsilon_2 > 0$  such that for all  $(m, n)$

$$\epsilon_1 \leq [\bar{\mathbf{W}}\bar{\mathbf{H}}]_{mn} \leq \epsilon_2. \quad (92)$$

Then, combining (83) with  $\sum_{m'} d_{mm'}^2 = 1$ , one can see that for all  $\Phi \in \mathcal{O}(M)$  and  $(m, n)$ ,

$$\epsilon_1 \leq \mathbb{E}([\Phi \mathbf{Y}]_{mn}^2) \leq \epsilon_2. \quad (93)$$

It follows that for any  $\epsilon > 0$

$$|\mathbb{E}_S([\Phi \mathbf{Y}]_{mn}^2) - \mathbb{E}([\Phi \mathbf{Y}]_{mn}^2)| < \epsilon, \quad (94)$$

$$\implies \left| \frac{\mathbb{E}_S([\Phi \mathbf{Y}]_{mn}^2) + \epsilon_0}{\mathbb{E}([\Phi \mathbf{Y}]_{mn}^2) + \epsilon_0} - 1 \right| < \frac{\epsilon}{\epsilon_0}, \quad (95)$$

and conversely

$$\left| \frac{\mathbb{E}_S([\Phi \mathbf{Y}]_{mn}^2) + \epsilon_0}{\mathbb{E}([\Phi \mathbf{Y}]_{mn}^2) + \epsilon_0} - 1 \right| < \epsilon, \quad (96)$$

$$\implies |\mathbb{E}_S([\Phi \mathbf{Y}]_{mn}^2) - \mathbb{E}([\Phi \mathbf{Y}]_{mn}^2)| < \epsilon(\epsilon_2 + \epsilon_0). \quad (97)$$

By definition of the convergence in probability, condition (30) is equivalent to:  $\forall \epsilon > 0$  and  $\delta \in (0, 1)$ , there exists  $S^*$  such that  $\forall S \geq S^*$

$$\Pr \left( \max_{m,n} \max_{\Phi \in \mathcal{O}(M)} |\mathbb{E}_S([\Phi \mathbf{Y}]_{mn}^2) - \mathbb{E}([\Phi \mathbf{Y}]_{mn}^2)| < \epsilon \right) > 1 - \delta, \quad (98)$$

which, using (94)–(95), implies that

$$\Pr \left( U_S < \frac{\epsilon}{\epsilon_0} \right) > 1 - \delta. \quad (99)$$

This proves that (30)  $\implies (U_S \xrightarrow{p} 0 \text{ as } S \rightarrow \infty)$ . The converse can be proven similarly with (96)–(97).

To complete the proof, it remains to show the inequality (91). First of all, let us notice that, from (8) and (92),  $\Sigma_n$  is positive definite and thus  $\Sigma_n^{-1/2}$  is well defined. Then, we have for all  $(m, n)$

$$\max_{\Phi \in \mathcal{O}(M)} \left| \frac{\mathbb{E}_S([\Phi \mathbf{Y}]_{mn}^2) + \epsilon_0}{\mathbb{E}([\Phi \mathbf{Y}]_{mn}^2) + \epsilon_0} - 1 \right| \quad (100)$$

$$\stackrel{(54)}{\leq} \max_{\phi \in \mathbb{R}^M: \|\phi\|_2=1} \left| \frac{\phi^\top (\Sigma_{n,S} - \Sigma_n) \phi}{\phi^\top \Sigma_n \phi} \right| \quad (101)$$

$$= \max_{\tilde{\phi} \in \mathbb{R}^M: \|\Sigma_n^{-1/2} \tilde{\phi}\|_2=1} \left| \frac{\tilde{\phi}^\top (\Sigma_n^{-1/2} \Sigma_{n,S} \Sigma_n^{-1/2} - \mathbf{I}) \tilde{\phi}}{\|\tilde{\phi}\|_2^2} \right| \quad (102)$$

$$= \max_{\tilde{\phi} \in \mathbb{R}^M: \|\tilde{\phi}\|_2=1} \left| \tilde{\phi}^\top (\Sigma_n^{-1/2} \Sigma_{n,S} \Sigma_n^{-1/2} - \mathbf{I}) \tilde{\phi} \right| \quad (103)$$

$$= \|\Sigma_n^{-1/2} \Sigma_{n,S} \Sigma_n^{-1/2} - \mathbf{I}\|, \quad (104)$$

which completes the proof.  $\square$

In Lemma 6, we show that  $\max_{\Phi \in \mathcal{O}(M)} Q_S(\Phi)$  (defined in (29)) can be controlled in terms of  $U_S$  and that it converges to 0 as  $U_S$  tends to 0.

**Lemma 6.** *Let  $U_S$  be defined as in Lemma 5. Then,*

$$U_S < 1 \implies \max_{\Phi \in \mathcal{O}(M)} Q_S(\Phi) \leq MN \frac{U_S^2}{1 - U_S}. \quad (105)$$

*Proof.* Let us first recall that

$$Q_S(\Phi) = \sum_{m,n=1}^{M,N} f \left( \frac{\mathbb{E}_S([\Phi \mathbf{Y}]_{mn}^2) + \epsilon_0}{\mathbb{E}([\Phi \mathbf{Y}]_{mn}^2) + \epsilon_0} \right), \quad (106)$$

for  $f(x) = x - \log(x) - 1$ . Then, by definition of  $U_S$  in (90) we have that, for all  $\Phi \in \mathcal{O}(M)$  and  $(m, n)$ ,

$$\frac{\mathbb{E}_S([\Phi \mathbf{Y}]_{mn}^2) + \epsilon_0}{\mathbb{E}([\Phi \mathbf{Y}]_{mn}^2) + \epsilon_0} \in [1 - U_S, 1 + U_S]. \quad (107)$$

Hence, because  $\forall x > 0, f(x) \leq g(x) := x + 1/x - 2$ , it follows from (106) and (107) that, if  $U_S < 1, \forall \Phi \in \mathcal{O}(M)$

$$Q_S(\Phi) \leq \sum_{m,n=1}^{M,N} g \left( \frac{\mathbb{E}_S([\Phi \mathbf{Y}]_{mn}^2) + \epsilon_0}{\mathbb{E}([\Phi \mathbf{Y}]_{mn}^2) + \epsilon_0} \right) \quad (108)$$

and thus

$$\max_{\Phi \in \mathcal{O}(M)} Q_S(\Phi) \leq MN \max_{x \in [1-U_S, 1+U_S]} g(x) \quad (109)$$

$$= MN \max\{g(1 - U_S), g(1 + U_S)\} \quad (110)$$

$$= MN g(1 - U_S) = MN \frac{U_S^2}{1 - U_S}. \quad (111)$$

Equality (110) comes from the fact that  $g$  is a convex function and (111) is due to  $g(1 - U_S) \geq g(1 + U_S)$  for  $U_S \in [0, 1)$ .  $\square$

### B. Proof of Theorem 3

The proof of Theorem 3 is a direct consequence of Lemmas 5 and 6. Indeed, under condition (30), we get from Lemma 5 that, for all  $\epsilon \in (0, \epsilon_0)$  and  $\delta \in (0, 1)$ , there exists  $S^*$  such that

$$S \geq S^* \implies \Pr\left(U_S < \frac{\epsilon}{\epsilon_0}\right) > 1 - \delta. \quad (112)$$

(cf. (99)) which, with Lemma 6, completes the proof.

### C. Proof of Theorem 4

From Lemma 5, showing that condition (30) is satisfied under GCM amounts to prove that under GCM we have  $U_S \xrightarrow{P} 0$  as  $S \rightarrow \infty$ . Moreover, by making explicit a bound on the convergence rate of  $U_S$ , we will get a bound on the convergence rate of  $\max_{\Phi \in \mathcal{O}(M)} Q_S(\Phi)$  thanks to Lemma 6.

According to Lemma 5 (Equation (91)), to show the convergence of  $U_S$  in probability, it is sufficient to show that each eigenvalue of  $\Sigma_n^{-1/2} \Sigma_{n,S} \Sigma_n^{-1/2}$  converges to one for each  $n$ .

To that end, let us first remark that the normalized matrix  $\Sigma_n^{-1/2} \Sigma_{n,S} \Sigma_n^{-1/2}$  can be regarded as an empirical covariance matrix obtained from the  $S$  “whitened” vectors  $\{\mathbf{x}_n^{(s)} = \Sigma_n^{-1/2} \mathbf{y}_n^{(s)}\}_{s=1}^S$ , i.e.,

$$\Sigma_n^{-1/2} \Sigma_{n,S} \Sigma_n^{-1/2} = \frac{1}{S} \sum_{s=1}^S \mathbf{x}_n^{(s)} \mathbf{x}_n^{(s)\top} = \mathbf{A}_S^\top \mathbf{A}_S, \quad (113)$$

where  $\mathbf{A}_S = \frac{1}{\sqrt{S}} [\mathbf{x}_n^1 \cdots \mathbf{x}_n^S]^\top \in \mathbb{R}^{S \times M}$ . Because the  $\mathbf{x}_n^{(s)}$  are i.i.d. realizations of a whitened Gaussian distribution whose covariance matrix is the identity, we obtain from [31, Corollary 5.35] that, for any  $t > 0$

$$\Pr(1 - \delta_S \leq \sigma_{\min}(\mathbf{A}_S) \leq \sigma_{\max}(\mathbf{A}_S) \leq 1 + \delta_S) \geq 1 - 2e^{-t^2/2}, \quad (114)$$

where  $\delta_S = \frac{\sqrt{M+t}}{\sqrt{S}}$  and  $\sigma_{\max}(\mathbf{A}_S)$  (resp.  $\sigma_{\min}(\mathbf{A}_S)$ ) denotes the largest (resp. smallest) singular value of  $\mathbf{A}_S$ . Using [31, Lemma 5.36], we get from (114) that

$$\Pr(\|\mathbf{A}_S^\top \mathbf{A}_S - \mathbf{I}\| \leq h_S) \geq 1 - 2e^{-t^2/2}, \quad (115)$$

with  $h_S := 3 \max(\delta_S, \delta_S^2)$ . Then, from (113),

$$\|\Sigma_n^{-1/2} \Sigma_{n,S} \Sigma_n^{-1/2} - \mathbf{I}\| = \|\mathbf{A}_S^\top \mathbf{A}_S - \mathbf{I}\|. \quad (116)$$

Combining the latter with (115), we obtain

$$\Pr\left(\|\Sigma_n^{-1/2} \Sigma_{n,S} \Sigma_n^{-1/2} - \mathbf{I}\| \leq h_S\right) \geq 1 - 2e^{-t^2/2}. \quad (117)$$

It follows, using the fact that the vectors  $\{\mathbf{x}_n^{(s)}\}_{s=1}^S$  are independent of the vectors  $\{\mathbf{x}_{n'}^{(s)}\}_{s=1}^S$  for  $n \neq n'$ , that

$$\begin{aligned} \Pr(U_S \leq h_S) &\geq \prod_{n=1}^N \Pr\left(\|\Sigma_n^{-1/2} \Sigma_{n,S} \Sigma_n^{-1/2} - \mathbf{I}\| \leq h_S\right) \\ &\geq (1 - 2e^{-t^2/2})^N, \end{aligned} \quad (118)$$

which proves that, under GCM,  $U_S \xrightarrow{P} 0$  as  $S \rightarrow \infty$ .

Finally, for  $t > 0$  and  $S$  large enough such that  $h_S = 3\delta_S < 1$ , we deduce from (118) and Lemma 6 that

$$\Pr\left(\max_{\Phi \in \mathcal{O}(M)} Q_S(\Phi) \leq MN \frac{h_S^2}{1 - h_S}\right) \quad (119)$$

$$\geq \Pr(U_S \leq h_S) \geq (1 - 2e^{-t^2/2})^N. \quad (120)$$

## APPENDIX F

### PROOFS OF PROPOSITIONS 3 AND 4

#### A. Optimality Conditions of Problem (37)

In order to prove Propositions 3 and 4, we first explicit the optimality conditions of the quadratic problem (37).

**Lemma 7.** *Let  $\Upsilon$  be the set of anti-symmetric matrices and  $\tilde{\mathcal{H}}$  be positive semi-definite. Then,  $\mathbf{E} \in \Upsilon$  is solution of problem (37) if and only if  $\mathbf{E} = (\mathbf{M} - \mathbf{M}^\top)/2$  with  $\mathbf{M} \in \mathbb{R}^{M \times M}$  solution of*

$$\frac{1}{4} \sum_{cd} [\mathcal{Z}]_{abcd} \left[ \frac{\mathbf{M} - \mathbf{M}^\top}{2} \right]_{cd} = -[\mathbf{G}^{(\text{anti})}]_{ab} \quad (121)$$

where  $[\mathcal{Z}]_{abcd} = [\tilde{\mathcal{H}}]_{abcd} + [\tilde{\mathcal{H}}]_{cdab} + [\tilde{\mathcal{H}}]_{badc} + [\tilde{\mathcal{H}}]_{dcba}$ .

*Proof.* Using the parametrization of the anti-symmetric matrix  $\mathbf{E} = (\mathbf{M} - \mathbf{M}^\top)/2$ , solving the constrained problem (37) is equivalent to solving the unconstrained problem

$$\widehat{\mathbf{M}} = \arg \min_{\mathbf{M} \in \mathbb{R}^{M \times M}} J(\mathbf{M}) \quad (122)$$

with

$$J(\mathbf{M}) = \left\langle \mathbf{G}, \frac{\mathbf{M} - \mathbf{M}^\top}{2} \right\rangle + \frac{1}{2} \left\langle \frac{\mathbf{M} - \mathbf{M}^\top}{2} | \tilde{\mathcal{H}} | \frac{\mathbf{M} - \mathbf{M}^\top}{2} \right\rangle.$$

where we recall that  $\langle \cdot, \cdot \rangle$  and  $\langle \cdot | \cdot \rangle$  are defined after equation (36). Given that  $J$  is convex (as  $\tilde{\mathcal{H}}$  is positive semi-definite), we get from the first-order optimality conditions that  $\nabla J(\widehat{\mathbf{M}}) = \mathbf{0}$ .

Because  $\langle \mathbf{G}, \mathbf{M}^\top \rangle = \langle \mathbf{G}^\top, \mathbf{M} \rangle$ , the first term of  $J$  is equal to  $\langle \mathbf{G}^{(\text{anti})}, \mathbf{M} \rangle$  and its gradient is thus given by  $\mathbf{G}^{(\text{anti})}$ . To compute the gradient of the second term, let us first expand

$$\begin{aligned} \langle \mathbf{M} + \Delta | \tilde{\mathcal{H}} | \mathbf{M} + \Delta \rangle &= \langle \mathbf{M} | \tilde{\mathcal{H}} | \mathbf{M} \rangle + o(\|\Delta\|) \\ &\quad + \langle \mathbf{M} | \tilde{\mathcal{H}} | \Delta \rangle + \langle \Delta | \tilde{\mathcal{H}} | \mathbf{M} \rangle. \end{aligned} \quad (123)$$

Then, by definition of the inner product, we get

$$\begin{aligned} \langle \Delta | \tilde{\mathcal{H}} | \mathbf{M} \rangle &= \sum_{ab} [\Delta]_{ab} \sum_{cd} [\tilde{\mathcal{H}}]_{abcd} [\mathbf{M}]_{cd}, \\ \langle \mathbf{M} | \tilde{\mathcal{H}} | \Delta \rangle &= \sum_{ab} [\Delta]_{ab} \sum_{cd} [\tilde{\mathcal{H}}]_{cdab} [\mathbf{M}]_{cd}. \end{aligned}$$

Similar expressions can be obtained when transposing one or both variables of the bilinear form in (123). We finally deduce from these expansions that

$$\begin{aligned} \left[ \nabla \langle \cdot | \tilde{\mathcal{H}} | \cdot \rangle (\mathbf{M}) \right]_{ab} &= \sum_{cd} ([\tilde{\mathcal{H}}]_{abcd} + [\tilde{\mathcal{H}}]_{cdab}) [\mathbf{M}]_{cd} \\ \left[ \nabla \langle (\cdot)^\top | \tilde{\mathcal{H}} | \cdot \rangle (\mathbf{M}) \right]_{ab} &= \sum_{cd} ([\tilde{\mathcal{H}}]_{cdab} + [\tilde{\mathcal{H}}]_{badc}) [\mathbf{M}^\top]_{cd} \\ \left[ \nabla \langle \cdot | \tilde{\mathcal{H}} | (\cdot)^\top \rangle (\mathbf{M}) \right]_{ab} &= \sum_{cd} ([\tilde{\mathcal{H}}]_{abcd} + [\tilde{\mathcal{H}}]_{dcba}) [\mathbf{M}^\top]_{cd} \\ \left[ \nabla \langle (\cdot)^\top | \tilde{\mathcal{H}} | (\cdot)^\top \rangle (\mathbf{M}) \right]_{ab} &= \sum_{cd} ([\tilde{\mathcal{H}}]_{badc} + [\tilde{\mathcal{H}}]_{dcba}) [\mathbf{M}]_{cd} \end{aligned}$$



Combining all these expressions, we obtain that  $\nabla J(\widehat{\mathbf{M}}) = \mathbf{0}$  is equivalent to (121), which completes the proof.  $\square$

### B. Proof of Proposition 3

By injecting the expression of  $[\tilde{\mathcal{H}}]_{abcd} = \delta_{ac}\delta_{bd}[\Gamma]_{ab}$  into (121) we get, for all  $(a, b)$ ,

$$[\Gamma^{(\text{sym})}]_{ab} \left[ \frac{\mathbf{M} - \mathbf{M}^\top}{2} \right]_{ab} = -[\mathbf{G}^{(\text{anti})}]_{ab}. \quad (124)$$

If, for a couple  $(a, b)$ , we have  $[\Gamma^{(\text{sym})}]_{ab} = 0$ , we get from the definition of  $\Gamma$  in (42) that  $\forall(n, s), [\mathbf{X}^{(s)}]_{bn} = 0$ . It follows from (40) that  $[\mathbf{G}]_{ab} = 0$  and thus that  $[\mathbf{G}^{(\text{anti})}]_{ab} = 0$ . Hence, for all  $(a, b)$  such that  $[\Gamma^{(\text{sym})}]_{ab} = 0$ , fixing  $\left[ \frac{\mathbf{M} - \mathbf{M}^\top}{2} \right]_{ab}$  to any real is solution of (124). In this work we choose the value 0 (second line in (43)). For all  $(a, b)$  such that  $[\Gamma^{(\text{sym})}]_{ab} \neq 0$ , we get from (124) the expression given in the first line in (43).

Finally, let us show that the optimal solution is a descent-direction, i.e.,  $\langle \mathbf{G}, \mathbf{E} \rangle < 0$ . From the definition of  $\Gamma$ , we get that  $[\Gamma^{(\text{sym})}]_{ab} \geq 0$ . Moreover, for all  $(a, b)$  such that  $[\Gamma^{(\text{sym})}]_{ab} = 0$  we fixed  $[\mathbf{E}]_{ab} = 0$ . Therefore,

$$\langle \mathbf{G}, \mathbf{E} \rangle = \langle \mathbf{G}^{(\text{anti})}, \mathbf{E} \rangle = - \sum_{\substack{(a,b) \\ [\mathbf{E}]_{ab} \neq 0}} \frac{[\mathbf{G}^{(\text{anti})}]_{ab}^2}{\Gamma_{ab}^{(\text{sym})}} < 0. \quad (125)$$

### C. Proof of Proposition 4

Again, by injecting the expression of

$$[\tilde{\mathcal{H}}]_{abcd} = \delta_{ac}\delta_{bd}[\Gamma]_{ab} + \delta_{ad}\delta_{bc} - 2\delta_{abcd}. \quad (126)$$

into (121) we obtain, for all  $(a, b)$ ,

$$([\Gamma^{(\text{sym})}]_{ab} - 1) \left[ \frac{\mathbf{M} - \mathbf{M}^\top}{2} \right]_{ab} = -[\mathbf{G}^{(\text{anti})}]_{ab}. \quad (127)$$

If, for a couple  $(a, b)$ , we have  $[\Gamma^{(\text{sym})}]_{ab} = 1$ , we get from the definition of  $\Gamma$  in (47) that  $\forall n, \frac{[\Phi(\sum_{n,S+\epsilon_0} \mathbf{I})\Phi^\top]_{bb}}{[\Phi(\sum_{n,S+\epsilon_0} \mathbf{I})\Phi^\top]_{aa}} = 1$ . It follows from (45) that  $[\mathbf{G}]_{ab} = [\mathbf{G}]_{ba}$  and thus that  $[\mathbf{G}^{(\text{anti})}]_{ab} = 0$ . Hence, for all  $(a, b)$  such that  $[\Gamma^{(\text{sym})}]_{ab} = 1$ , fixing  $\left[ \frac{\mathbf{M} - \mathbf{M}^\top}{2} \right]_{ab}$  to any real number is solution of (127). In this work we choose the value 0 (second line in (48)). For all  $(a, b)$  such that  $[\Gamma^{(\text{sym})}]_{ab} \neq 1$ , we get from (127) the expression given in the first line in (48).

Finally, let us show that the optimal solution is a descent-direction, i.e.,  $\langle \mathbf{G}, \mathbf{E} \rangle < 0$ . From the definition of  $\Gamma$ , we get that  $[\Gamma^{(\text{sym})}]_{ab} \geq 1$ . Moreover, for all  $(a, b)$  such that  $[\Gamma^{(\text{sym})}]_{ab} = 1$  we fixed  $[\mathbf{E}]_{ab} = 0$ . Therefore,

$$\langle \mathbf{G}, \mathbf{E} \rangle = \langle \mathbf{G}^{(\text{anti})}, \mathbf{E} \rangle = - \sum_{\substack{(a,b) \\ [\mathbf{E}]_{ab} \neq 0}} \frac{[\mathbf{G}^{(\text{anti})}]_{ab}^2}{\Gamma_{ab}^{(\text{sym})} - 1} < 0. \quad (128)$$

## APPENDIX G MULTI-INITIALIZATION STRATEGY

We describe a multi-initialization strategy that allows to obtain numerical solutions that are close to the solution sets  $\Omega^*$  and  $\Omega^\bullet$ . To that end, we first consider  $P$  random initializations

$$\{(\Phi_0^{(p)}, \mathbf{W}_0^{(p)}, \mathbf{H}_0^{(p)})\}_{p \leq P} \quad (129)$$

from which we run the TL-NMF and JD+NMF solvers in Algorithms 1 and 2. Given an initialization, each method is run for  $J$  iterations. In order to robustify the process, the solutions obtained with JD+NMF (resp. TL+NMF)  $\{(\Phi_J^{(p)}, \mathbf{W}_J^{(p)}, \mathbf{H}_J^{(p)})\}_{p \leq P}$  are used as extra  $P$  initializations

$$\{(\Phi_0^{(p)}, \mathbf{W}_0^{(p)}, \mathbf{H}_0^{(p)})\}_{P+1 \leq p \leq 2P} \quad (130)$$

for TL-NMF (resp. JD+NMF). Finally, for TL-NMF, we preserve only the solution  $(\hat{\Phi}^*, \hat{\mathbf{W}}^*, \hat{\mathbf{H}}^*)$  that achieves the smallest  $C_S$ . For JD+NMF, we preserve only the solution  $\hat{\Phi}^\bullet$  that achieves the smallest  $L_S$ . We then minimize  $I_S(\hat{\Phi}^\bullet, \cdot, \cdot)$ , started from  $\{(\mathbf{W}_0^{(p)}, \mathbf{H}_0^{(p)})\}_{p \leq 2P}$ , and preserve the best solution  $(\hat{\mathbf{W}}^\bullet, \hat{\mathbf{H}}^\bullet)$  that achieves the smallest loss  $I_S$ .

## REFERENCES

- [1] A. Berman and R. J. Plemmons, *Nonnegative matrices in the mathematical sciences*. SIAM, 1994.
- [2] C. Févotte, N. Bertin, and J. L. Durrieu, "Nonnegative matrix factorization with the Itakura-Saito divergence: With application to music analysis," *Neural Computation*, vol. 21, no. 3, pp. 793–830, mar 2009.
- [3] P. Smaragdis, C. Févotte, G. J. Mysore, N. Mohammadiha, and M. Hoffman, "Static and dynamic source separation using nonnegative factorizations: A unified view," *IEEE Signal Processing Magazine*, vol. 31, no. 3, pp. 66–75, may 2014.
- [4] D. Fagot, H. Wendt, and C. Févotte, "Nonnegative matrix factorization with transform learning," in *Proc. ICASSP*, Calgary, Canada, 2018, pp. 2431–2435.
- [5] S. Zhang, E. Soubies, and C. Févotte, "On the identifiability of transform learning for non-negative matrix factorization," *IEEE Signal Processing Letters*, vol. 27, pp. 1555–1559, 2020.
- [6] K. Yoshii, K. Kitamura, Y. Bando, E. Nakamura, and T. Kawahara, "Independent low-rank tensor analysis for audio source separation," in *European Signal Processing Conference*, vol. 2018-Sept, Roma, Italy, 2018, pp. 1657–1661.
- [7] E. Vincent, T. Virtanen, and S. Gannot, *Audio source separation and speech enhancement*. John Wiley & Sons, 2018.
- [8] S. Makino, *Audio source separation*. Springer, 2018.
- [9] N. Gillis, *Nonnegative Matrix Factorization*. SIAM, 2020.
- [10] S. Ravishanker and Y. Bresler, "Learning Sparsifying Transforms," *IEEE Transactions on Signal Processing*, vol. 61, no. 5, pp. 1072–1086, mar 2013.
- [11] A. Hyvärinen, J. Karhunen, and E. Oja, *Independent Component Analysis*. John Wiley & Sons, 2001.
- [12] P. Comon and C. Jutten, *Handbook of blind source separation*. Academic press, 2010.
- [13] X. Fu, K. Huang, N. D. Sidiropoulos, and W.-K. Ma, "Nonnegative Matrix Factorization for Signal and Data Analytics: Identifiability, Algorithms, and Applications," *IEEE Signal Processing Magazine*, vol. 36, no. 2, pp. 59–80, 2019.
- [14] D. T. Pham and J.-F. Cardoso, "Blind separation of instantaneous mixtures of nonstationary sources," *IEEE Transactions on Signal Processing*, vol. 49, no. 9, pp. 1837–1848, sep 2001.
- [15] F. Itakura and S. Saito, "Analysis synthesis telephony based on the maximum likelihood method," in *International Congress on Acoustics*, Los Alamitos, CA, USA, 1968, pp. 17–20.
- [16] X. Fu, K. Huang, and N. D. Sidiropoulos, "On identifiability of nonnegative matrix factorization," *IEEE Signal Processing Letters*, vol. 25, no. 3, pp. 328–332, 2018.
- [17] O. Ledoit and M. Wolf, "A well-conditioned estimator for large-dimensional covariance matrices," *Journal of Multivariate Analysis*, vol. 88, no. 2, pp. 365–411, feb 2004.
- [18] J.-F. Cardoso and A. Souloumiac, "Jacobi angles for simultaneous diagonalization," *SIAM Journal on Matrix Analysis and Applications*, vol. 17, no. 1, pp. 161–164, jan 1996.
- [19] J.-F. Cardoso, "On the performance of orthogonal source separation algorithms," in *Proc. EUSIPCO*, Edinburgh, Scotland, sep. 1994, pp. 776–779.
- [20] D. T. Pham, "Joint approximate diagonalization of positive definite Hermitian matrices," *SIAM Journal on Matrix Analysis and Applications*, vol. 22, no. 4, pp. 1136–1152, may 2001.



- [21] A. Yeredor, “Non-orthogonal joint diagonalization in the least-squares sense with application in blind source separation,” *IEEE Transactions on Signal Processing*, vol. 50, no. 7, pp. 1545–1553, jul 2002.
- [22] A. Ziehe, P. Laskov, G. Nolte, and K.-R. Müller, “A Fast Algorithm for Joint Diagonalization with Non-Orthogonal Transformations and Its Application to Blind Source Separation,” *Journal of Machine Learning Research*, vol. 5, no. 1, pp. 777–800, jul 2004.
- [23] P.-A. Absil and K. A. Gallivan, “Joint Diagonalization on the Oblique Manifold for Independent Component Analysis,” in *Proc. ICASSP*, Toulouse, France, 2006.
- [24] A. Souloumiac, “Nonorthogonal Joint Diagonalization by Combining Givens and Hyperbolic Rotations,” *IEEE Transactions on Signal Processing*, vol. 57, no. 6, pp. 2222–2231, mar 2009.
- [25] F. Bouchard, B. Afsari, J. Malick, and M. Congedo, “Approximate Joint Diagonalization with Riemannian Optimization on the General Linear Group,” *SIAM Journal on Matrix Analysis and Applications*, vol. 41, no. 1, pp. 152–170, jan 2020.
- [26] B. Afsari, “Sensitivity Analysis for the Problem of Matrix Joint Diagonalization,” *SIAM Journal on Matrix Analysis and Applications*, vol. 30, no. 3, pp. 1148–1171, sep 2008.
- [27] M. Kleinstueber and H. Shen, “Uniqueness Analysis of Non-Unitary Matrix Joint Diagonalization,” *IEEE Transactions on Signal Processing*, vol. 61, no. 7, pp. 1786–1796, jan 2013.
- [28] N. Takahashi, J. Katayama, M. Seki, and J. Takeuchi, “A unified global convergence analysis of multiplicative update rules for nonnegative matrix factorization,” *Computational Optimization and Applications*, vol. 71, no. 1, pp. 221–250, mar 2018.
- [29] L. T. K. Hien and N. Gillis, “Algorithms for Nonnegative Matrix Factorization with the Kullback–Leibler Divergence,” *Journal of Scientific Computing*, vol. 87, no. 3, p. 93, may 2021.
- [30] C. Févotte and J. Idier, “Algorithms for nonnegative matrix factorization with the  $\beta$ -divergence,” *Neural Computation*, vol. 23, no. 9, pp. 2421–2456, sep 2011.
- [31] R. Vershynin, “Introduction to the non-asymptotic analysis of random matrices,” in *Compressed Sensing: Theory and Applications*. Cambridge University Press, 2012, pp. 210–268.
- [32] ———, *High-Dimensional Probability: An Introduction with Applications in Data Science*. Cambridge University Press, 2018.
- [33] Y. Sun, P. Babu, and D. P. Palomar, “Majorization-minimization algorithms in signal processing, communications, and machine learning,” *IEEE Transactions on Signal Processing*, vol. 65, no. 3, pp. 794–816, 2017.
- [34] P. Ablin, J.-F. Cardoso, and A. Gramfort, “Beyond Pham’s algorithm for joint diagonalization,” in *Proc. ESANN*, Bruges, Belgium, 2019, pp. 607–612.
- [35] P. Ablin, D. Fagot, H. Wendt, A. Gramfort, and C. Févotte, “A quasi-Newton algorithm on the orthogonal manifold for NMF with transform learning,” in *Proc. ICASSP*, Brighton, United Kingdom, 2019, pp. 700–704.
- [36] H. Wendt, D. Fagot, and C. Févotte, “Jacobi algorithm for nonnegative matrix factorization with transform learning,” in *European Signal Processing Conference*, vol. 2018-Sept, Roma, Italy, 2018, pp. 1062–1066.
- [37] J. H. Manton, “Optimization algorithms exploiting unitary constraints,” *IEEE Transactions on Signal Processing*, vol. 50, no. 3, pp. 635–650, aug 2002.
- [38] P. Wolfe, “Convergence Conditions for Ascent Methods,” *SIAM Review*, vol. 11, no. 2, pp. 226–235, apr 1969.